PKCδ is an activator of neuronal mitochondrial metabolism that mediates the spacing effect on memory consolidation

Authors

Typhaine Comyn[1], Thomas Preat[1], Alice Pavlowsky[1,2,*] and Pierre-Yves Plaçais[1,2,*]

Affiliations

[1]Energy & Memory, Brain Plasticity Unit, CNRS, ESPCI Paris, PSL Research University, 10 rue Vauquelin, 75005 Paris, France.

[2]Co-corresponding authors

*Correspondence: alice.pavlowsky@espci.fr; pierre-yves.placais@espci.fr

Abstract

Relevance-based selectivity and high energy cost are two distinct features of long-term memory (LTM) formation that warrant its default inhibition. Spaced repetition of learning is a highly conserved cognitive mechanism that can lift this inhibition. Here, we questioned how the spacing effect integrates experience selection and energy efficiency at the cellular and molecular levels. We showed in Drosophila that spaced training triggers LTM formation by extending over several hours an increased mitochondrial metabolic activity in neurons of the associative memory center, the mushroom bodies (MBs). We found that this effect is mediated by PKCδ, a member of the so-called 'novel PKC' family of enzymes, which uncovers the critical function of PKCδ in neurons as a regulator of mitochondrial metabolism for LTM. Additionally, PKCδ activation and translocation to mitochondria result from LTM-specific dopamine signaling on MB neurons. By bridging experience-dependent neuronal circuit activity with metabolic modulation of memory-encoding neurons, PKCδ signaling binds the cognitive and metabolic constraints underlying LTM formation into a unified gating mechanism.

MAIN TEXT

Introduction

Long-term memory (LTM) is a fundamental cognitive process that allows organisms to efficiently retain and retrieve information over extended (and sometimes lifelong) periods of time. Since the long-term retention of fortuitous or poorly relevant associations can drive maladaptive behavior, the triage of learning experiences and routing to LTM has to be tightly gatekept. As a result of this cognitive constraint, brains have evolved mechanisms for the default inhibition of LTM formation (Abel et al., 1998; Scheunemann et al., 2018). Under certain circumstances, LTM inhibition is lifted in a process known as LTM gating. Defective gating in either direction is expected to cause memorization deficits or (on the contrary) hypermnesia, with both conditions leading to a severe deterioration in the quality of life. It is therefore crucial to decipher the underlying mechanisms behind this precisely regulated process. One of the most conserved conditions known to potently lift the default inhibition of LTM formation is the spaced repetition of learning (Abel et al., 1998; Shaughnessy, 1977), which has been reported in a number of species from *Aplysia* (Sutton et al., 2002), *C. elegans* (Nishijima and Maruyama, 2017) and Drosophila (Tully et al., 1994) to mice (Glas et al., 2021) and humans (Shaughnessy, 1977). This phenomenon is called the spacing effect, in contrast with intensive learning (or cramming), in which massed presentation of information leads to the formation of a less persistent form of consolidated memory (Shaughnessy, 1977). Studies in animal models, in particular in fruit flies using an associative aversive olfactory paradigm, demonstrated that LTM formation following spaced training exerts a significant energetic burden on organisms (Mery and Kawecki, 2005; Padamsey and Rochefort, 2023; Plaçais et al., 2017; Plaçais and Preat, 2013). Following the paired delivery of an odorant with electric shocks, flies show learned avoidance of this odorant for a couple hours (Quinn et al., 1974). Whereas spaced repetition of odor/shock pairing allows sustained retention (up to one week) (Bouzaiane et al., 2015; Heisenberg, 2003), massed training results in the rapid decline (1-2 days) of the formed memory, which provides a powerful, experimentally tractable way to model the spacing effect versus cramming. Strikingly, in the hours following spaced training in fruit flies, their sucrose intake is observed to increase by over twofold (Plaçais et al., 2017), which does not occur after massed training. In addition, spaced, but not massed, training decreases the survival duration of flies under conditions of limited resources (Plaçais and Preat, 2013). These observations reveal a major impact of LTM formation on the energy balance of the whole organism, with this metabolic constraint being an additional incentive for the default inhibition

of LTM formation. Interestingly, the recent finding that cellular energy fluxes are involved in the control of LTM formation (Plaçais et al., 2017) suggests that both cognitive and metabolic constraints linked with LTM formation may be merged in a unitary, cost-effective gating process. Indeed, we previously showed that the upregulation of mitochondrial metabolic activity in neurons of the mushroom bodies (MB), the insect brain's memory center, in the first hours following spaced training is critical to initiating LTM formation (Plaçais et al., 2017). This upregulation of mitochondrial metabolism depends on post-learning dopamine signaling from a specific pair of MB-afferent neurons, called MP1 neurons (or PPL1-γ1pedc neurons (Aso et al., 2014)), which show sustained calcium rhythmic activity in the same time windows encompassing the first hours after spaced training (Plaçais et al., 2012). MP1 activates MB mitochondrial activity via the DAMB receptor (also named Dop1R2) (Plaçais et al., 2017). The putative interdependence of cognitive and metabolic constraints, two sides of the same coin, therefore calls for the identification of the neuronal molecular gatekeeper at the core of the spacing effect, linking neuronal network activity and mitochondrial energy metabolism.

The G-protein-coupled receptor DAMB preferentially engages with Gq (Cassar et al., 2015; Himmelreich et al., 2017), which signals via the second messengers DAG (Mizuno and Itoh, 2009) and calcium, two canonical activators of the broad family of PKC enzymes. One particular PKC isoform, PKCδ, that belongs to the 'novel' PKC class (Duquesnes et al., 2011) exclusively regulated by DAG but not calcium (Duquesnes et al., 2011), shows unique properties that make it a candidate of particular interest. In non-neuronal mammalian cells, it was shown that PKCδ can translocate to mitochondria upon its activation (Wu-zhang et al., 2012), where it specifically localizes to the intermembrane space. There, PKCδ is able to activate oxidative metabolism by targeting the pyruvate dehydrogenase (PDH) complex (Acin-Perez et al., 2010; Kim and Hammerling, 2020), which catalyzes the first step of pyruvate metabolism for oxidative phosphorylation. Despite this evidence, the mechanisms underlying the regulation of PKCδ translocation to mitochondria upon activation, and how it interfaces with extracellular signals, remains poorly understood. Although PKCδ expression is commonly used to identify specific neurons in the mammalian brain (Cai et al., 2014; Cui et al., 2017; Dilly et al., 2022; Haubensak et al., 2010; Wang et al., 2020; Williford et al., 2023), the functional role of PKCδ in brain tissues has remained thus far largely unexplored. Nonetheless, the putative ability of PKCδ to act as the interface between Gq-mediated activation and metabolic activity control prompted us to study this kinase as the missing piece in the puzzle of LTM gating that could bridge dopaminergic activation and neuronal mitochondrial metabolism.

We first uncovered that PKCδ activation is required in MB neurons for LTM formation through behavior experiments involving targeted genetic inhibition of PKCδ and *in vivo* functional brain imaging using a specific sensor of PKCδ activity, δCKAR (Kajimoto et al., 2010; Wu-zhang et al., 2012), which we introduced in Drosophila. We further showed that PKCδ is a downstream effector of DAMB and that its translocation to the mitochondria is triggered upon LTM formation by MP1/DAMB signaling. Employing *in vivo* imaging of cellular pyruvate consumption, we showed that PKCδ intervenes in LTM formation through its metabolic role as a mitochondrial activator, by releasing the pyruvate dehydrogenase (PDH) complex inhibition. We therefore revealed that a major effect of spaced training is to mobilize the DAMB/PKCδ signaling cascade in order to perpetuate for several hours a neuronal metabolic enhancement that only transiently occurs after a single learning session. Overall, our data establish PKCδ as an essential activator of neuronal pyruvate mitochondrial metabolism that mediates the spacing effect on memory consolidation.

Results

PKCδ is required in MB neurons for LTM formation

To investigate the role of PKCδ in memory, we downregulated PKCδ expression at the adult stage in the MB neurons (see schematic in Figure 1A) and assessed memory formed using different protocols of aversive olfactory conditioning. These different protocols include the single association between an odor and shocks (1x conditioning), which elicits a short-lived memory that will rapidly decay after a few hours; 5 spaced cycles of conditioning with 15 min of rest intervals (5x spaced), which induces LTM; and 5 massed presentations without pauses (5x massed), which leads to the formation of a less robust, cramming-like type of memory (Bouzaiane et al., 2015; Heisenberg, 2003; Tully et al., 1994). To spatially and temporally restrict PKCδ RNAi expression, we took advantage of the VT30559-Gal4 MB driver (Plaçais et al., 2017) combined with the ubiquitously expressed thermosensitive Gal4 inhibitor tub-Gal80^{ts} (McGuire et al., 2003). This system allows inducing RNAi expression in the MBs of adult flies, by transferring them at 30°C two days before conditioning. This protocol successfully decreased the whole-head PKCδ mRNA level (Figure 1B), thereby revealing PKCδ expression in MB neurons. When PKCδ was knocked down in adult MB neurons, flies subjected to 5x spaced conditioning presented LTM impairment (Figure 1C). When flies of the same genotype were kept at 18°C prior to conditioning, i.e. without induction of RNAi

expression, LTM was normal (Figure 1C). In addition, the sensitivity to shocks and odors was normal in induced flies (Supplementary Table 1). We then investigated if other types of aversive memory were also affected by PKCδ knockdown in adult MB neurons. No defect was detected when memory was measured 24 h after 5x massed conditioning (Figure 1C), and memory was not affected when tested 3 h after single-cycle training (Figure 1C). All of these results were replicated with a second non-overlapping RNAi against PKCδ (Figure 1 – figure supplement 1A), which downregulates PKCδ expression with similar efficiency (Figure 1 – figure supplement 1B). Altogether, these series of experiments demonstrate that PKCδ is specifically required for LTM in adult MB neurons, fulfilling the first condition for a molecular effector of the spacing effect.

Next, we investigated whether PKCδ was activated in MB neurons following spaced training. We took advantage of the existence of a genetically encoded FRET-based fluorescent reporter of PKCδ-specific activity, δCKAR (Kajimoto et al., 2010; Wu-zhang et al., 2012), and generated Drosophila lines carrying this sensor under UAS control. Expression of the δCKAR sensor in the adult MB neurons was achieved using the tub-Gal80^{ts};VT30559-Gal4 driver as for the behavior experiments. To assess the efficacy of the δCKAR sensor in Drosophila neurons, we first used two-photon *in vivo* imaging in the MB vertical lobes of naïve flies to monitor the response of the δCKAR sensor to pharmacological activation of PKCδ, using PDBu (Wu-zhang et al., 2012). PDBu application induced a robust response of the sensor as compared to solvent alone (Figure 1D). Because PDBu can activate other PKCs than PKCδ (Alzamora et al., 2007; Wu-zhang et al., 2012), we ascertained the specificity of this response by performing the same experiment in flies expressing PKCδ RNAi in the MB at the adult stage, where PDBu failed to elicit a δCKAR response as compared to flies that do not carry PKCδ RNAi (Figure 1E). Notably, the order of magnitude of the maximum δCKAR response (2-3%) is consistent with what was previously measured *in cellulo* (Wu-zhang et al., 2012).

Having established the responsiveness and the specificity of the δCKAR sensor, we sought to use this tool to measure the PKCδ activity level after conditioning in the MB vertical lobes, which are privileged sites of LTM encoding (Pascual and Préat, 2001; Séjourné et al., 2011; Yu et al., 2006). To compare post-conditioning PKCδ activity between different protocols, δCKAR traces were normalized to the plateau value reached after saturation of the sensor by addition of PDBu, so that the activity level of PKCδ in each individual fly could be estimated as a δCKAR signal value before PDBu application (Figure 1F). Measurements were performed in a time window of 30 min to 1 h 30 min after the end of training, when increased mitochondrial

metabolism in MB vertical lobes after 5x spaced was previously reported (Plaçais et al., 2017; Rabah et al., 2022). Using this procedure, we observed that the PKCδ activity level was increased following spaced training, as compared to control flies that were submitted to a non-associative unpaired spaced protocol (Figure 1F). Importantly, the PKC substrate-uncompetitive inhibitor Bis IV (Wu-zhang et al., 2012) (Figure 1 – figure supplement 1C) was still able to induce a decrease in PKCδ activity after spaced training (Figure 1 – figure supplement 1D), ruling out the alternative hypothesis that lack of a PDBu-induced δCKAR response following spaced training might stem from an inhibition of PKCδ expression or a decrease of its activity below the detection threshold of the δCKAR sensor. Therefore, we conclude from our results that 5x spaced conditioning actually induced a marked enhancement of PKCδ activity in MB neurons. In addition, neither massed nor 1x training elicited such an increase in PKCδ activity levels (Figure 1G-H), which supports the specific effect of spaced conditioning on PKCδ activation and is consistent with the outcome of our behavioral experiments.

The specific requirement of PKCδ in LTM formation prompted us to investigate whether it was more particularly required in α/β neurons of the MB, one of the three anatomical categories of MB neurons and a subpopulation known to be pivotal in LTM encoding (Pascual and Préat, 2001; Séjourné et al., 2011; Yu et al., 2006). We therefore restricted PKCδ RNAi expression to the α/β neurons exclusively at the adult stage, by means of the tub-Gal80^{ts};c739-Gal4 inducible driver (Turrel et al., 2018). This strongly impaired LTM performance after spaced training (Figure 2A). When RNAi expression was not induced, LTM was normal (Figure 2A). Naïve odor and shock avoidance were unaffected by PKCδ knockdown in adult α/β neurons (Supplementary Table 1). Neither 3-h memory after 1x training (Figure 2A) nor memory after massed training were impaired (Figure 2 – figure supplement 1A). Hence, we show that PKCδ is more specifically required in α/β neurons for LTM formation. We then investigated PKCδ activity after spaced conditioning more specifically in α/β MB neurons using the δCKAR sensor. Consistent with the requirement of PKCδ specifically for LTM in the α/β neurons, we observed an increase in PKCδ post-training activity after spaced conditioning (Figure 2B), an activation that was not elicited by a single-cycle of training (Figure 2C).

Altogether, we demonstrate here that PKCδ is specifically activated after spaced training and is required for LTM formation in MB α/β neurons, placing it as a key player of the spacing effect.

PKCδ regulates mitochondrial pyruvate metabolism for LTM

We have shown that PKCδ activation occurs after spaced training concomitantly to the increased mitochondrial metabolic activity that is known to be critical for the initiation of LTM formation (Plaçais et al., 2017). As PKCδ can modulate mitochondrial metabolism in other tissues (Acin-Perez et al., 2010; Kim and Hammerling, 2020), we wondered whether PKCδ activation in neurons was involved in this process. To address this question, we first asked whether pharmacological PKCδ activation using PDBu in a naïve context could be sufficient to upregulate the mitochondrial pyruvate flux in MB neurons. To this end, we used *in vivo* two-photon imaging of the genetically encoded pyruvate sensor Pyronic (San Martín et al., 2014) expressed in all MB neurons. We employed a previously characterized protocol (Plaçais et al., 2017) to obtain a dynamic measurement of the pyruvate flux to mitochondria, by measuring the slope of pyruvate accumulation following the injection of sodium azide, a potent inhibitor of the mitochondrial respiratory chain (complex IV) (Figure 3 – figure supplement 1A). In the brains of naïve flies, activation of PKCδ through PDBu application resulted in an upregulated pyruvate flux to the mitochondria of the MB vertical lobes (Figures 3A and Figure 3 – figure supplement 1B). This upregulation did not occur when PKCδ was knocked down in adult MB neurons (Figures 3A and Figure 3 – figure supplement 1B), indicating that the increased pyruvate consumption relies on PKCδ activation by PDBu. These results reveal that in naïve flies, PKCδ activation is sufficient to increase the pyruvate flux to mitochondria in MB neurons.

We then investigated whether PKCδ mediates metabolic upregulation after spaced training. As previously reported (Plaçais et al., 2017), we observed an increased pyruvate flux in MB vertical lobes following spaced conditioning (Figure 3B) during the same time frame as for PKCδ activation. Remarkably, this effect was abolished by PKCδ knockdown in adult MB (Figure 3B). Therefore, we conclude that a critical role of PKCδ in LTM formation is to upregulate mitochondrial pyruvate metabolism for LTM gating.

Next, we examined how PKCδ could regulate mitochondrial pyruvate consumption. We previously showed that the upregulation of the pyruvate flux critical for LTM formation is directly related to the level of pyruvate dehydrogenase (PDH) activity (Plaçais et al., 2017). PDH activity is regulated by its level of phosphorylation: the PDH kinase (PDK) inhibits PDH, whereas PDH phosphatase (PDP) activates it (Lavington et al., 2014) (Figure 3C). Furthermore, in non-neuronal cells, PKCδ has been described as an inhibitor of PDK (Acin-Perez et al., 2010; Kim and Hammerling, 2020). Therefore, we hypothesized that a similar mechanism – i.e. PDK inhibition resulting in PDH activation – may occur in neurons in the context of LTM formation.

To test this hypothesis, we reasoned that genetic inhibition of PDK may alleviate the LTM defect elicited by PKCδ knockdown (as described in Figure 1C). Indeed, we observed that coexpression of PDK and PKCδ RNAis in adult α/β MB neurons did not induce a memory impairment, whereas expression of the PKCδ RNAi alone induced an LTM defect as expected (Figure 3C). Thus, inhibiting PDK is sufficient to fully rescue the memory defect induced by loss of PKCδ, showing that upregulating pyruvate flux is the critical function of PKCδ in LTM formation.

MP1 neurons activate PKCδ in the mitochondria of MB neurons via DAMB signaling

As detailed in the introduction, the metabolic upregulation induced by spaced training has been shown to be triggered by early post-learning activity of MP1 dopamine neurons, through the Gq-coupled DAMB receptor (Plaçais et al., 2017). We therefore asked if MP1 neuronal dopamine signaling through the DAMB receptor could activate PKCδ and induce its mitochondrial translocation, which would be detected as an increase in PKCδ activity specifically at the level of the mitochondria. For this, we expressed a mitochondria-addressed δCKAR sensor, mito-δCKAR (Figure 4 – figure supplement 1), in MB neurons, and monitored PKCδ activity while artificially activating MP1 neurons in naïve flies using dTrpA1, a heat-sensitive cation channel that allows to induce neuronal firing through acute temperature increase (Hamada et al., 2008; Plaçais et al., 2012). At the level of the peduncle, where MP1 neurons project on to the α/β MB neurons (Aso et al., 2014) (Figure 4A), flies subjected to the activation of MP1 neurons showed an increased PKCδ mitochondrial activity as compared to flies that received a similar thermal treatment but did not express dTrpA1 (Figure 4B). Strikingly, in flies that were additionally knocked down for the DAMB receptor in the MBs, MP1 neuron activation failed to increase PKCδ mitochondrial activity (Figure 4B). Interestingly, we found that PKCδ mitochondrial activity could also be increased in the vertical lobes of the MB in response to MP1 activation (Figure 4C). Altogether, these data show that DAMB signaling from MP1 neurons triggers increased PKCδ mitochondrial activity, reflecting its translocation to mitochondria in MB neurons.

To explore whether PKCδ mitochondrial activation and translocation occur upon 5x spaced conditioning for LTM formation, we expressed the mito-δCKAR sensor in α/β neurons and measured PKCδ activity after 5x spaced training, using the same method as in Figure 1F-H. At the level of the peduncle, we found that 5x spaced training elicited a marked increase in PKCδ mitochondrial activity, as compared to the corresponding unpaired protocol (Figure 5A).

Remarkably, DAMB knockdown in adult α/β neurons hampered PKCδ activation in mitochondria after 5x spaced training (Figure 5A). We observed a similar DAMB-dependent effect at the level of the vertical lobes (Figure 5B). Altogether, our data show that MP1-DAMB signaling induced by spaced conditioning results in PKCδ activation at the level of the mitochondria, where it upregulates the PDH complex to gate LTM formation through increased pyruvate flux.

Spaced training prolongs learning-induced metabolic enhancement

The results obtained thus far uncover a DAMB/PKCδ cascade that mediates an increase in pyruvate consumption by MB neuronal mitochondria. As previously reported (Rabah et al., 2022), single-cycle training also induces a metabolic upregulation of similar magnitude, typically observed 1-2 h after training. However, we observed that the metabolic enhancement induced by single-cycle training (Figure 6A) faded away rapidly, as it was no longer detectable 3 hours after 1x training (Figure 6B). Moreover, the metabolic upregulation occurring after 1x training was not dependent on DAMB signaling (Figure 6C), nor did it require PKCδ activity in MB neurons (Figure 6D), contrary to what was observed after spaced training (see Plaçais et al., 2017 for DAMB and Figure 3B for PKCδ). This led us to hypothesize that the role of this DAMB/PKCδ cascade after spaced training is to extend the duration of the metabolic enhancement in MB neurons. Indeed, measurements performed 3-4 hours as well as 8-9 hours after the last cycle of spaced training (i.e. respectively 5-6 hours and 10-11 hours after the end of the first training cycles) revealed that increased metabolic activity was still occurring (Figure 6E-F). In contrast, measurements performed 24 hours after spaced training showed that the metabolic enhancement had stopped by that time point (Figure 6G). Altogether, our results demonstrate that spaced training specifically recruits dopamine/DAMB/PKCδ signaling to perpetuate the metabolic activation in MB neurons, which is critical for initiating LTM formation (Figure 7).

Discussion

In this study, we unveiled a detailed molecular mechanism underlying the spacing effect on memory consolidation. We established that PKCδ, a known regulator of mitochondrial pyruvate metabolism in several peripheral tissues, is a critical player in LTM formation in α/β MB neurons, while being dispensable for less stable forms of aversive memory. Additionally, we

imported in Drosophila a genetically-encoded FRET sensor for PKCδ (Kajimoto et al., 2010; Wu-zhang et al., 2012), which allowed observing the PKCδ activity level *in vivo*. Thus, we reported a specific activation and mitochondrial translocation of PKCδ following spaced training, but not 1x or massed training. We established that specific dopaminergic neurons (MP1 neurons), which are required early after spaced training for LTM formation (Plaçais et al., 2017, 2012), activate PKCδ translocation to mitochondria, through a specific Gq-coupled dopamine receptor, DAMB. Consistent with the role of this dopamine signaling that we previously reported (Plaçais et al., 2017), we showed here that activated PKCδ persistently upregulates pyruvate metabolism, thereby allowing LTM formation. Altogether, our data demonstrate that PKCδ, acting as an activator of mitochondrial metabolism, is a neuronal gatekeeper of LTM formation. More generally, our findings provide a detailed mechanistic description of how dopamine signaling orchestrates memory consolidation through sustained modulation of neuronal energy fluxes, thereby resolving within a single gating mechanism the cognitive and metabolic constraints linked to LTM formation.

Although PKCs have been widely implicated in learning and memory in a large variety of model organisms (Van Der Zee and Douma, 1997), the precise contribution of PKCδ in memory formation and consolidation in mammals remains largely unknown. Nevertheless, PKCδ is highly expressed in brain regions associated with learning, and more specifically aversive learning and memory (Zafiri and Duvarci, 2022). In particular, it is found in the CA3 layer of the hippocampus, as well as in a specific region of the central nucleus of the amygdala (CeA) called CE1 (Haubensak et al., 2010) *(see also http://mouse.brain-map.org)*. There, PKCδ marks about 50% of CEl GABAergic neurons (Haubensak et al., 2010). Strikingly, it was shown that CeA is implicated in learning and consolidation of Pavlovian fear conditioning (Steinberg et al., 2020; Wilensky et al., 2006), and more specifically that PKCδ+ neurons of the CeA projecting to the substantia innominata (SI) bidirectionally modulate negative reinforcement learning (Cui et al., 2017). However, no link between the function of PKCδ itself and memory consolidation or metabolism has been established yet, as the PKCδ-expressing feature of these neurons was only used as a means to genetically target them in the aforementioned studies. Our work thus sketches a possibly conserved role of neuronal PKCδ in the context of memory formation and consolidation in mammals, which nevertheless remains to be investigated. A possible role of PKCδ in plasticity mechanisms in mice was substantiated by the recent observation, in CA1 pyramidal neurons from mice organotypic slices, that stimulation-induced DAG production downstream of NMDA receptors (Colgan et al., 2018) can activate PKCδ in

spines for local plasticity, and, at a longer timescale, its translocation to the nucleus for plasticity-induced transcription upon LTP formation (Colgan et al., 2023).

How is post-learning dopamine signaling coupled with PKCδ activation? DAMB is a dopamine receptor that has the ability to activate Gq with great efficiency and dopamine sensitivity (Himmelreich et al., 2017), which results in the production of DAG, a canonical activator of the majority of PKC enzymes. Once activated by DAG, the local hydrophobic patch generated by DAG fixation is thought to guide PKCs to various membranes (Hurley and Grobler, 1997), and notably to mitochondria in the case of PKCδ where it localizes to the intermembrane space (Acin-Perez et al., 2010; Kim and Hammerling, 2020). In addition, PKCδ is specific among PKCs in that it does not require activation loop phosphorylation for catalytic competence (Duquesnes et al., 2011). This direct link between DAG and PKCδ (and the absence of any requirement for PKCδ phosphorylation) may explain its physiological role as an efficient relay between extracellular cues sensed by receptors and intracellular metabolism at the level of the mitochondria. DAMB/Gq can also activate calcium signaling (Cassar et al., 2015; Himmelreich et al., 2017), the other canonical second-messenger pathway downstream of Gq. Since increases in mitochondrial calcium flux are another way to enhance PDH complex activity (Denton et al., 1972; Glancy and Balaban, 2012), one cannot exclude that mitochondrial calcium signaling may also play a role in the gating mechanism for LTM formation.

Gq/PKC signaling has also been shown to play a major role in memory in rodents. Mutation in the phosphosite of TrkB that binds phospholipase C (PLC) to produce DAG and activate PKC signaling impaired expression and maintenance of synaptic long-term potentiation in the hippocampus, and overall reduced learning in mice (Gruart et al., 2007; Minichiello et al., 2002). Thus, the Gq-DAG mechanism of PKCδ activation for memory consolidation could be conserved in mammals. While DAMB has no direct homology with mammalian dopaminergic receptors (instead belonging to an “invertebrate type” class of receptors as demonstrated by sequence comparison (Mustard et al., 2005)), it should be noted that several mammalian dopamine receptors are also known to mobilize Gq signaling, such as the D1-D2 and the D5-D2 dopamine receptor heteromers (So et al., 2009; Young and Thomas, 2014). D1-like receptor can also directly engage with Gq/11 and therefore PLC (Rashid et al., 2007). In mammals, this non-canonical D1-like receptor/Gq coupling was notably found in the hippocampus and amygdala (Jin et al., 2001; Ming et al., 2006), two brain areas that are enriched in PKCδ+ neurons (Haubensak et al., 2010; Zafiri and Duvarci, 2022). Anatomical studies demonstrate that both D1 and D2 receptors are expressed in the CeA, a region of the brain enriched in PKCδ+

neurons (Zafiri and Duvarci, 2022). Periaqueductal gray/dorsal raphe (PAG/DR) afferent dopaminergic neurons exhibit phasic activation in response to an aversive unconditioned stimulus (US) and to a conditioned stimulus (CS) associated with the aversive US (Groessl et al., 2018; Zafiri and Duvarci, 2022), which could preferentially activate the D1 receptor-expressing CeA neurons during aversive learning (Zafiri and Duvarci, 2022). It would be of particular interest to explore the involvement of PKCδ neurons in this process, and to study whether PKCδ could be mobilized downstream of D1/Gq signaling in the context of aversive memory in mammals. Aside from dopaminergic receptors, a wide variety of memory-relevant receptors have been reported to activate Gq signaling, with adrenergic receptors being the most commonly cited kind. In physiological conditions, α-adrenergic receptors are considered to be the principal activators of Gq signaling (Duquesnes et al., 2011). β-adrenoreceptor subtypes are expressed in the hippocampus and amygdala; these regions receive noradrenergic afferences from the locus coeruleus, which plays a critical role in regulating behavioral memory in rodents, and are key for the processing of memories (Sara, 2009), and more specifically for their consolidation (Sara, 2009; Souza-Braga et al., 2018).

Here, we propose a model in which a state of high energy consumption in MB neuron axons necessary for LTM gating is prolonged by PKCδ, which boosts the PDH complex activity in MB mitochondria. Such a role is consistent with previous descriptions in non-neuronal mammalian cells. It is indeed known that PKCδ can regulate the PDH complex (Acin-Perez et al., 2010; Kim and Hammerling, 2020): activation of PKCδ leads to the phosphorylation of a putative PDK phosphatase, thereby enhancing its activity and promoting dephosphorylation of PDK, which inhibits it and thereby releases the inhibition it exerts on the PDH complex (Acin-Perez et al., 2010; Kim and Hammerling, 2020). As PDK knockdown rescued the LTM defect induced by PKCδ knockdown in our study, we propose that PKCδ boosts the PDH complex activity via this mechanism of PDK-Pase activation, resulting in PDK inhibition in MB neuronal mitochondria. This lasting effect of PKCδ on mitochondrial metabolism thus maintains the pyruvate flux upregulated in MB vertical lobe mitochondria, which unlocks memory consolidation to form LTM.

While our work uncovers a molecular switch controlling the metabolic upregulation of the MB neurons, the role for this enhanced pyruvate flux to mitochondria has not yet been unveiled. Several hypotheses could be considered, which are not mutually exclusive. First, increased pyruvate incorporation into the TCA cycle could lead to acceleration of oxidative phosphorylation and subsequent enhanced ATP production, in support of sustained neuronal

activity or of the substantial energy cost of *de novo* protein synthesis on which LTM formation depends at later stages (Davis and Squire, 1984; Helmstetter et al., 2008; Jarome and Helmstetter, 2014). Second, acceleration of the TCA cycle and oxidative phosphorylation can also be accompanied by increased ROS production (Rosato et al., 2014), both of which are increasingly recognized as neuronal signaling molecules (Sinenko et al., 2021; Zhang et al., 2016). Third, acceleration of the TCA cycle alone, decoupled from oxidative phosphorylation, could produce acetylcholine, the neurotransmitter used by MB neurons, and/or acyl groups that are crucial for subsequent epigenetic modifications. This non-canonical TCA cycle has recently been reported in a model of mammalian stem cells (Arnold et al., 2022). Finally, TCA cycle intermediates could be used for amino acid synthesis to fulfill the need for *de novo* protein synthesis, which is a hallmark of LTM.

Our study extends to the context of memory formation in neurons the beneficial role of PKCδ in the modulation of mitochondrial metabolism, whereas it was first extensively described in the mouse embryonic fibroblast (Acin-Perez et al., 2010). There, PKCδ serves as an indispensable supervisor of mitochondrial energy production: by sensing the cytochrome c redox state as a proxy of the respiratory chain workload, it adjusts mitochondrial metabolism within safe margins (that can be overpassed when fuel flux surpasses the capacity of the electron-transport chain, causing detrimental ROS release) (Acin-Perez et al., 2010; Kim and Hammerling, 2020). Strikingly, PKCδ was also widely described as detrimental to cells in pathological conditions, with a well-characterized role in cardiac (Inagaki et al., 2003; Zaja et al., 2014) and neuronal (Bright et al., 2004; Dave et al., 2011; Phan et al., 2002) cell death upon ischemic incidents. In this model, PKCδ takes part in apoptotic events through a caspase-induced signaling cascade in mitochondria, notably via cleavage by caspase-3 at the PKCδ caspase-dependent cleavage site, which releases a 40 kDa active fragment. Furthermore, transient episodes of ischemia can also activate PKCδ through ROS-dependent mechanisms, leading to its phosphorylation and subsequent activation. PKCδ can then bind and phosphorylate Drp1, a major mitochondrial fission protein, thereby increasing its activity. This mechanism was described in cardiomyocytes during anoxia-reoxygenation injury (Zaja et al., 2014), and in neurons under oxidative stress *in cellulo*, as well as *in vivo* in the context of hypertension-induced encephalopathy (Qi et al., 2011). Finally, PKCδ has been implicated in neurodegenerative diseases such as Alzheimer's disease (AD) (Du et al., 2018) and Parkinson's disease (PD) (Kaul et al., 2005; Yang et al., 2004; Zhang et al., 2007). However, a number of these studies should be considered carefully, as some of their results are based on PKCδ

inhibition by rottlerin, which has been found to be an inappropriate and ineffective PKCδ pharmacological inhibitor (Soltoff, 2007). Nevertheless, various pieces of evidence show increased expression of PKCδ in AD patients (Du et al., 2018), pointing towards the fact that PKCδ inhibition plays an important protective role in brain aging (Conboy et al., 2009), ischemia (Bright et al., 2004; Dave et al., 2011; Phan et al., 2002), and neurodegenerative disease (Du et al., 2018; Kaul et al., 2005; Yang et al., 2004; Zhang et al., 2007).

Altogether, it is now emerging that PKCδ is functionally ambivalent: while its role in metabolism regulation maintains essential physiological functions such as LTM gating in the brain as demonstrated in this study, stress conditions unveil negative effects mediated by this kinase that derail the system equilibrium. The interplay between the two modes of activation of PKCδ by DAG and oxidative stress is probably at the heart of its contrasting duality. Expanding upon our work, it could be of particular interest to explore whether competition between PKCδ activation via these two modes, DAG and oxidative stress, occurs upon aging and/or pathology.

Material and Methods

RESOURCE AVAILABILITY

Materials availability

Materials generated in this study are available from the corresponding authors without restriction.

Data and code availability

All data needed to evaluate the conclusions are present in the manuscript and/or the Supplementary Information. Data reported in this manuscript will be shared by the corresponding authors upon request. Any additional information required to reanalyze the data reported in this manuscript is available from the corresponding authors upon request.

Key resources table

REAGENT or RESOURCE	SOURCE	IDENTIFIER
Chemicals, peptides, and recombinant proteins		
3-octanol (99%)	Sigma-Aldrich	Cat. #153095
4-methylcyclohexanol (98%)	Sigma-Aldrich	Cat. #218405
Paraffine GPR Rectapur	VWR	Cat. #24679.360

NaCl	Sigma-Aldrich	Cat. #S9625
KCl	Sigma-Aldrich	Cat. #P3911
$MgCl_2$	Sigma-Aldrich	Cat. #M9272
$CaCl_2$	Sigma-Aldrich	Cat. #C3881
D-trehalose	Sigma-Aldrich	Cat. #9531
Sucrose	Sigma-Aldrich	Cat. #S9378
HEPES-NaOH	Sigma-Aldrich	Cat. #H7637
Phorbol 12,13-dibutyrate (PdBu)	Tocris	Cat. #4153
Bisindolylmaleimide IV (Bis IV)	Sigma-Aldrich	Cat. #B3306
Sodium Azide	Sigma-Aldrich	Cat. #71289
Critical commercial assays		
RNeasy Plant Mini Kit	QIAGEN	Cat. #74904
RNA MinElute Cleanup Kit	QIAGEN	Cat. #74204
SuperScript III First-Strand Kit	Thermofisher Invitrogen	Cat. #18080-051
SYBR Green I Master mix	Roche	Cat. # 04729692001
Experimental models: Organisms/strains		
tubulin-Gal80^{ts};VT30559-Gal4	Plaçais et al., 2017	
tubulin-Gal80^{ts};c739-Gal4	Turrel et al., 2018	
tubulin-Gal80^{ts};elav-Gal4	Silva et al., 2022	
30E11-LexA	BDSC	#54209
UAS-PKCδ$^{RNAi\ JF02991}$	BDSC	#28355
UAS-PKCδ$^{RNAi\ KK109117}$	VDRC	#101421
UAS-DAMB$^{RNAi\ KK110947}$	VDRC	#105324
UAS-PDK$^{RNAi\ KK106641}$	VDRC	#106641
LexAop-dTrpA1	Liu et al., 2012	N/A
tubulin-Gal80^{ts};VT30559-Gal4, UAS-Pyronic	Plaçais et al., 2017	N/A
30E11-LexA;VT30559-Gal4	Plaçais et al., 2017	N/A
UAS-cyto-δCKAR;UAS-PKCδ$^{RNAi\ JF01991}$	This paper	N/A
UAS-mito-δCKAR;UAS-DAMB$^{RNAi\ KK110947}$	This paper	N/A
UAS-mito-δCKAR;UAS-DAMB$^{RNAi\ KK110947}$;LexAop-dTrpA1	This paper	N/A
UAS-PDK$^{RNAi\ KK106641}$;UAS-PKCδ$^{RNAi\ JF02991}$	This paper	N/A
UAS-mtDsRed	BDSC	#93056
Oligonucleotides		
Primer PKCδ forward: 5'-GGCACCAAACACCCGTATCT-3'	This paper, DRSC Fly Primer Bank	Primer Pair PP14953
Primer PKCδ reverse: 5'-CCCATAGAATCTGGCTCGCT-3'	This paper, DRSC Fly Primer Bank	Primer Pair PP14953
Primer tub forward: 5'-TTGTCGCGTGTGAAACACTTC-3'	Turrel et al., 2018	N/A
Primer tub reverse: 5'-CTGGACACCAGCCTGACCAAC-3'	Turrel et al., 2018	N/A
Recombinant DNA		
pcDNA3-deltaCKAR	Addgene	#31526
pJFRC-MUH	Addgene	#26213
pJRFC-MUH-UAS-deltaCKAR	This paper	
pJRFC-MUH-UAS-delta mitoCKAR	This paper	

EXPERIMENTAL MODEL AND SUBJECT DETAILS

D. melanogaster flies were maintained on standard cornmeal-yeast-agar medium. Stocks were kept at 18°C and 60% humidity under a 12-hour light:12-hour dark cycle. Genetic crosses were

performed at 18°C for behavior experiments or at 23°C for imaging experiments (except when indicated otherwise). Both male and female flies were used for behavior experiments. Female flies were used for imaging experiments due to their larger size. Flies from the Vienna Drosophila Resource Center (VDRC) collection were outcrossed for 5 generations to a reference strain carrying the w^{1118} mutation in an otherwise Canton Special (Canton S) genetic background. Since TRiP RNAi transgenes do not carry a mini-white marker but are labeled with a y^+ marker, flies from the TRiP RNAi collection were outcrossed to a y^1w^{67c23} strain in an otherwise Canton S background. The Canton S strain was used as the wild type strain.

To target MB neurons, the VT30559-Gal4 line was used in combination with the thermosensitive TARGET system tubulin-Gal80^{ts} to generate the tub-Gal80^{ts};VT30559-Gal4 inducible driver line (Plaçais et al., 2017), so as to temporally control the expression of the desired transgene. Gal4 activity was released by transferring 0- to 2-day-old adult flies to 30°C for 2-3 days. Likewise, the c739-Gal4 line was used to specifically target α/β neurons, and the tubulin-Gal80^{ts};c739-Gal4 construct line previously generated in the laboratory and described in Turrel et al., 2018 allowed temporal control of the Gal4 activity. As described in Silva et al., 2022, the tubulin-Gal80^{ts};elav-Gal4 system was used for time-controlled pan-neuronal knockdown. To target MP1 neurons independently of the Gal4 system, the 30E11-LexA driver was used (Plaçais et al., 2017). The tub-Gal80^{ts}; VT30559-Gal4, UAS-Pyronic line was previously generated in our research group and described in Plaçais et al., 2017. The UAS-cyto-δCKAR and UAS-mito-δCKAR lines were generated for this study (see 'Generation of transgenic flies' section below). The following genetic constructs were generated in this study by combining the appropriate UAS-RNAi line (listed in the key resources table) and FRET sensor transgenes: i) UAS-cyto-δCKAR;UAS-PKCδ$^{RNAi\ JF01991}$, ii) UAS-mito-δCKAR;UAS-DAMB$^{RNAi\ KK110947}$, iii) UAS-mito-δCKAR;UAS-DAMB$^{RNAi\ KK110947}$;LexAop-dTrpA1, and iv) UAS-PDK$^{RNAi\ KK106641}$; UAS-PKCδ$^{RNAi\ JF02991}$. All other fly lines used in this study are listed in the key resources table and either come from the VDRC collection or TRiP RNAi collection, or were previously published.

METHOD DETAILS

Aversive olfactory conditioning and memory test. The behavioral experiments, including sample sizes, were conducted similarly to previous studies from our research group (Plaçais et al., 2017; Scheunemann et al., 2018). For all experiments, training and testing were performed in a sound- and odor-proof room at 25°C and 80% humidity. Experimental flies (male and

female) were transferred to fresh bottles containing standard medium on the day before conditioning for the non-induced condition. For the induced condition, flies were transferred 2 days before the experiment at 30.5°C to allow RNAi expression.

Conditioning. Flies were conditioned by exposure to one odor paired with electric shocks and subsequent exposure to a second odor in the absence of shock. A barrel-type machine was used for simultaneous automated conditioning of six groups of 40–50 flies each. Throughout the conditioning protocol, each barrel was attached to a constant air flow at 2 $L.min^{-1}$. The odorants 3-octanol (odor O) and 4-methylcyclohexanol (odor M), diluted in paraffin oil at 0.360 and 0.325 mM respectively, were alternately used as conditioned stimuli (CS). For a single cycle of associative training, flies were first exposed to an odorant (the CS+) for 1 min while 12 pulses of 5 s-long, 60 V electric shocks were delivered; flies were then exposed 45 s later to a second odorant without shocks (the CS–) for 1 min. Here, the groups of flies were subjected to one of the following olfactory conditioning protocols: 1 cycle training (1x), five consecutive associative training cycles (5x massed training), or five associative cycles spaced by 15-min inter-trial intervals (5x spaced conditioning). Non-associative control protocols (unpaired protocols) were also employed for *in vivo* imaging experiments. During unpaired conditionings, the odor and shock stimuli were delivered separately in time, with shocks occurring 3 min before the first odorant. After training and until memory testing, flies were kept on regular food at 25°C (for 3 h-memory test) or at 18°C (for 24 h memory test).

Memory test. The memory test was performed either 3 h after 1x conditioning or 24 h after 5x conditioning in a T-maze apparatus comprising a central elevator to transfer the flies to the center of the maze arms. During the test, flies were exposed simultaneously to both odors (the same concentration as during conditioning) in the T-maze. After 1 min of odorant exposure in the dark, flies were trapped in either T-maze arm, retrieved and counted. A memory score was calculated as the number of flies avoiding the conditioned odor minus the number of flies preferring the conditioned odor, divided by the total number of flies. A single memory score value is the average of two scores obtained from two groups of genotypically identical flies conditioned in two reciprocal experiments, using either odorant (3-octanol or 4-methylcyclohexanol) as the CS+. The indicated ‘n’ is the number of independent memory score values for each genotype.

Odor perception test. The olfactory acuity of flies was tested after conditioning with the CS+, since electric shocks modify their olfactory perceptions. Flies were then immediately tested in a T-maze, where they had to choose between the CS– or its solvent (paraffin oil). Odor

concentrations used in this assay were the same as for the memory assays. At these concentrations, both odorants are innately repulsive. The odor-interlaced side was alternated for successively tested groups. After 1 minute, flies were counted, and naïve odor avoidance was calculated as for the memory test.

Electric shock perception test. During the test, flies must choose between two barrels: one delivering the electric shocks, and one that is neutral. The compartment where the electric shocks are delivered was alternated between two consecutive groups. After 1 minute, flies were counted, and shock avoidance was calculated as for the memory test.

In vivo imaging. Crosses for imaging experiments were raised at 23°C and fly progeny were induced for three days at 30.5°C to drive sufficient expression of the probe (and the desired RNAi) for use in imaging, except for MP1 activation experiments involving the thermosensitive LexAop-dTrpA1 transgene in which flies were always kept at 18°C. As in all previous imaging work from our laboratory, all *in vivo* imaging was performed on female flies, which are preferred since their larger size facilitates surgery. Naïve (not trained) or conditioned flies (1x, 5x spaced or 5x massed and their corresponding unpaired controls) were gently handled by aspiration without anesthesia and glued on their dorsal side to a plastic coverslip coated with a thin transparent plastic sheet. The coverslip was then placed on a recording chamber. Surgery was performed to obtain an imaging window on the fly head by removing the cuticle, trachea and fat bodies, thereby exposing the underlying MB neurons. During the procedure, the head capsule is bathed in a drop of artificial hemolymph: NaCl 130 mM (Sigma cat. # S9625), KCl 5 mM (Sigma cat. # P3911), MgCl2 2 mM (Sigma cat. # M9272), CaCl2 2 mM (Sigma cat. # C3881), D-trehalose 5 mM (Sigma cat. # 9531), sucrose 30 mM (Sigma cat. # S9378), and HEPES hemisodium salt 5 mM (Sigma cat. # H7637). At the end of the procedure, any remaining solution was absorbed and a fresh 90-µL droplet was applied on the preparation. When performed on flies that underwent olfactory conditioning, the imaging experiments were performed within the time period after conditioning indicated on each figure panel.

FRET δCKAR imaging. Imaging was performed using a SP8 DIVE Leica 2-photon microscope equipped with a 25x, 1.0 NA water immersion objective. Two-photon excitation of CFP was achieved using an Insight X3 Spectra Physics laser tuned to 840 nm. 512x250 images were acquired at the rate of one image every two seconds, with two z plans imaged in parallel (vertical lobes and peduncle). Typically, the images comprised the structures of both brain hemispheres, although only one hemisphere was visible in some preparations. Two spectrally

tunable hybrid detectors were adjusted to detect 440-490 nm CFP emission and 510-550 nm YFP emission. Two minutes after the beginning of image acquisition, 10 µL of a 2.5 mM phorbol 12,13-dibutyrate (PDBu, Tocris cat. # 4153) solution (25 mM PDBu stock solution in DMSO dissolved at 1/10 in artificial hemolymph) were injected into the 90 µL-droplet bathing the fly's brain, bringing PDBu to a final concentration of 250 µM (DMSO: 1/100). In control experiments, PDBu injection was replaced by the injection of DMSO alone (final concentration: 1/100). To inhibit PKCδ, two minutes after the beginning of image acquisition, 10 µL of a 50 µM bisindolylmaleimide IV (Bis IV, Sigma cat. # B3306) solution (500 µM stock solution in DMSO dissolved at 1/10 in artificial hemolymph), bringing Bis IV to a final concentration of 5 µM. In control experiments, Bis IV injection was replaced by the injection of DMSO alone (final concentration: 1/100). Drug application during the recording could give rise to artifactual perturbation of the signal at the time of injection, with variability from one experiment to another. In Figure 1F, a section of the presented traces corresponding to the 15 seconds following the injection was smoothed using a running average procedure (with a time window of 30 s) to remove injection artefacts that were especially large in this initial series of experiments. The injection technique was subsequently improved so that no smoothing was applied on any of the other presented experiments (including in particular Figure 2B, which reports a similar phenomenon as Figure 1F).

For image analysis, regions of interest (ROI) were delimited by hand around each visible vertical lobe or peduncle region, and the average intensity of both CFP and YFP channels over each ROI were calculated over time after background subtraction; the background was evaluated as the mean intensity over a region of interest placed in a nonfluorescent part of the brain. The δCKAR sensor was designed so that FRET from CFP to YFP decreases when PKCδ phosphorylating activity increases. The inverse FRET ratio, ΔR (CFP/YFP), was computed to obtain a signal that positively correlates with PKCδ phosphorylating activity. To measure the δCKAR response (Figure 1D-E, Figure 1 – figure supplement 1C-D, Figure 4), the ΔR ratio was normalized by a baseline value calculated over the 2 min preceding drug injection (PDBu or Bis IV). To measure PKCδ post-training activity (Figure 1F-H, Figure 2B-C, Figure 5), the ΔR ratio was normalized by a plateau value calculated from 6 min 40 s to the end of the recording, and the controls were normalized to 1.

For the MP1 activation experiments in which PKCδ response activity was assayed (Figure 4), flies were prepared as previously reported and placed on a custom-made device equipped with a Peltier cell to allow precise control of the temperature under the microscope. Flies were

recorded for 2 min at 18°C to establish a baseline and then received thermal treatment for MP1 activation, consisting of three consecutive periods of 2 min at 30°C followed by 2 min at 18°C. The recording was continued for 10 min after the last activation period. To measure PKCδ response activity, the ΔR was normalized by the baseline value calculated over the 2 min preceding thermal treatment, and the controls were normalized to 1.

The indicated 'n' is the number of animals that were assayed in each condition.

FRET imaging of pyruvate flux. Two-photon imaging was performed using a Leica TCS-SP5 upright microscope equipped with a 25x, 0.95 NA water immersion objective. Two-photon excitation was achieved using a Mai Tai DeepSee laser tuned to 825 nm. The frame rate was two images per second. 512x150 images were acquired at a rate of two images per second. The emission channels for mTFP and Venus were the same as described in Gervasi et al., 2010. Measurements of pyruvate consumption were performed according to a previously well-characterized protocol (Plaçais et al., 2017). After 1 min of baseline acquisition, 10 µL of a 50 mM sodium azide solution (Sigma cat. #71289; prepared in the same artificial hemolymph solution) were injected into the 90 µL-droplet bathing the fly's brain, bringing sodium azide to a final concentration of 5 mM. In experiments involving pretreatment of the brains (Figure 3A), 250 µM of PDBu or 1/100 DMSO (final concentrations) were injected into the hemolymph droplet 3 minutes prior to sodium azide injection. Image analysis was performed as previously described (Plaçais et al., 2017). ROI were delimited by hand around each visible MB vertical lobe, and the average intensity of the mTFP and Venus channels over each ROI was calculated over time after background subtraction. The Pyronic sensor was designed so that FRET from mTFP to Venus decreases when the pyruvate concentration increases. To obtain a signal that positively correlates with pyruvate concentration, the inverse FRET ratio was computed as mTFP intensity divided by Venus intensity. This ratio was normalized by a baseline value calculated over the 1 min preceding drug injection. The slope was calculated between 10 and 70% of the plateau. The indicated 'n' is the number of animals that were assayed in each condition.

RT-qPCR analyses. To assess the efficiency of the PKCδ RNAi used in this study, female flies carrying the tubulin-Gal80^{ts};elav-Gal4 pan-neuronal inducible driver were either crossed with UAS-PKCδ RNAi JF02991 or UAS-PKCδ KK109117 males, or with CS males for controls (please note that crosses of these RNAi lines with the constitutive elav-Gal4 driver were lethal for the progeny). To assess PKCδ presence in the MB neurons, female flies carrying the tubulin-

Gal80^{ts};VT30559-Gal4 MB neuron driver were either crossed with UAS-PKCδ RNAi JF02991 males, or with CS males for controls. Fly progeny were raised at 23°C throughout their development. Newly hatched flies were transferred to fresh food vials at 30.5°C for 4 days of induction before RNA extraction, as previously reported (Silva et al., 2022). RNA extraction and cDNA synthesis were performed using the RNeasy Plant Mini Kit (Qiagen), RNA MinElute Cleanup Kit (Qiagen), oligo(dT)20 primers and the SuperScript III First-Strand kit (Thermo Fisher Invitrogen). Amplification was performed using a LightCycler 480 (Roche) and the SYBR Green I Master mix (Roche). Specific primers used for PKCδ cDNA and the refence α-Tub84B (Tub, CG1913) cDNA are specified in the key resources table. The level of PKCδ cDNA was compared against the level of the α-Tub84B reference cDNA. Each reaction was performed in triplicate. The specificity and size of amplification products were assessed by melting curve analyses. Expression relative to the reference was presented as the foldchange compared to the calibrator (relative quantification RQ = $2^{-\Delta\Delta Ct}$, where Ct is the cycle threshold).

Generation of transgenic flies. To generate the UAS-cyto-δCKAR line, the pcDNA3-deltaCKAR plasmid (Addgene #31526) was digested by HindIII and XbaI. The resulting fragment was purified by electrophoresis and cloned into a pJFRC-MUH plasmid (Addgene #26213) in the XbaI/NotI subcloning site. The resulting construct was verified by restriction analysis and sequenced by PCR. This subcloning was outsourced to RDBiotech (France). The UAS-mito-δCKAR line was generated using the plasmid mito-δCKAR generated in Wu-zhang et al., 2012 by subcloning the mito-δCKAR fragment (HindIII/XbaI) into the pJFRC-MUH plasmid. The generation of the transgenic fly strains via the embryonic injection of the two vectors was outsourced to Rainbow Transgenic Flies, Inc (CA, USA).

QUANTIFICATION AND STATISTICAL ANALYSIS

Statistical parameters including the definitions and exact value of n, deviations and P values are reported in the figures and corresponding legends. Data are expressed as the mean ± SEM with dots as individual values corresponding to either a group of 40–50 flies analyzed together in a behavioral assay, or the response of a single recorded fly for imaging. Statistical analysis and graphs were made using Prism 8 (GraphPad software, v8.4.3). Comparisons between 2 groups were performed using a two-tailed unpaired t-test; results are provided as the value t_x of the t distribution with x degrees of freedom obtained from the data. Comparisons between multiple groups were performed using one-way ANOVA followed by Tukey's post hoc test for pairwise

comparisons. ANOVA results are given as the value of the Fisher distribution $F_{x,y}$ obtained from the data, where x is the numerator degrees of freedom and y is the denominator degrees of freedom. Asterisks denote the smallest significant difference between the relevant group and its controls with the post hoc comparisons (*p<0.05, **p<0.01, ***p<0.001, ****p<0.0001, ns: not significant).

Acknowledgments

We thank the TRiP consortium at Harvard Medical School (NIH/NIGMS R01-GM084947) and the BDSC and VDRC fly stock centers for providing transgenic RNAi fly stocks, and Eloïse de Trédern for help in subcloning the mito-δCKAR plasmid. We are also grateful to Dr Jaime de Juan-Sanz for insightful comments on the manuscript. The authors acknowledge funding from the European Research Council (ERC Advanced Grant EnergyMemo n°741550, to T.P.), from the Agence Nationale de la Recherche (ANR, to P.-Y.P) and from DIM ELICIT's grant from Région Ile-de-France (equipment grant, to P.-Y.P). T.C. was funded by a doctoral fellowship from the French Ministry of Research.

Author contributions

Conceptualization: all authors
Methodology: T.C., A.P., P.-Y.P.
Investigation: T.C.
Writing—original draft: T.C., A.P., P.-Y.P.
Writing—review & editing: all authors
Funding: T.P., P.-Y.P.

Competing interests

The authors declare no competing interests.

References

Abel T, Martin KC, Bartsch D, Kandel ER. 1998. Memory Suppressor Genes: Inhibitory Constraints on the Storage of Long-Term Memory. *Science* **279**:338–341. doi:10.1126/science.279.5349.338

Acin-Perez R, Hoyos B, Gong J, Vinogradov V, Fischman DA, Leitges M, Borhan B, Starkov A, Manfredi G, Hammerling U. 2010. Regulation of intermediary metabolism by the PKCδ signalosome in mitochondria. *The FASEB Journal* **24**:5033–5042. doi:10.1096/fj.10-166934

Alzamora R, Brown LR, Harvey BJ. 2007. Direct Binding and Activation of Protein Kinase C Isoforms by Aldosterone and 17β-Estradiol. *Molecular Endocrinology* **21**:2637–2650. doi:10.1210/me.2006-0559

Arnold PK, Jackson BT, Paras KI, Brunner JS, Hart ML, Newsom OJ, Alibeckoff SP, Endress J, Drill E, Sullivan LB, Finley LWS. 2022. A non-canonical tricarboxylic acid cycle underlies cellular identity. *Nature* **603**:477–481. doi:10.1038/s41586-022-04475-w

Aso Y, Hattori D, Yu Y, Johnston RM, Iyer NA, Ngo TTB, Dionne H, Abbott LF, Axel R, Tanimoto H, Rubin GM. 2014. The neuronal architecture of the mushroom body provides a logic for associative learning. *eLife* **3**:e04577. doi:10.7554/eLife.04577

Bouzaiane E, Trannoy S, Scheunemann L, Plaçais PY, Preat T. 2015. Two Independent Mushroom Body Output Circuits Retrieve the Six Discrete Components of Drosophila Aversive Memory. *Cell Reports* **11**:1280–1292. doi:10.1016/j.celrep.2015.04.044

Bright R, Raval AP, Dembner JM, Pérez-Pinzón MA, Steinberg GK, Yenari MA, Mochly-Rosen D. 2004. Protein Kinase C δ Mediates Cerebral Reperfusion Injury In Vivo. *J Neurosci* **24**:6880–6888. doi:10.1523/JNEUROSCI.4474-03.2004

Cai H, Haubensak W, Anthony TE, Anderson DJ. 2014. Central amygdala PKC-δ(+) neurons mediate the influence of multiple anorexigenic signals. *Nat Neurosci* **17**:1240–1248. doi:10.1038/nn.3767

Cassar M, Issa AR, Riemensperger T, Petitgas C, Rival T, Coulom H, Iché-Torres M, Han KA, Birman S. 2015. A dopamine receptor contributes to paraquat-induced neurotoxicity in Drosophila. *Human Molecular Genetics* **24**:197–212. doi:10.1093/hmg/ddu430

Colgan LA, Hu M, Misler JA, Parra-Bueno P, Moran CM, Leitges M, Yasuda R. 2018. PKCα integrates spatiotemporally distinct Ca2+ and autocrine BDNF signaling to facilitate synaptic plasticity. *Nat Neurosci* **21**:1027–1037. doi:10.1038/s41593-018-0184-3

Colgan LA, Parra-Bueno P, Holman HL, Tu X, Jain A, Calubag MF, Misler JA, Gary C, Oz G, Suponitsky-Kroyter I, Okaz E, Yasuda R. 2023. Dual Regulation of Spine-Specific and Synapse-to-Nucleus Signaling by PKCδ during Plasticity. *J Neurosci* **43**:5432–5447. doi:10.1523/JNEUROSCI.0208-22.2023

Conboy L, Foley AG, O'Boyle NM, Lawlor M, Gallagher HC, Murphy KJ, Regan CM. 2009. Curcumin-induced degradation of PKCδ is associated with enhanced dentate NCAM PSA expression and spatial learning in adult and aged Wistar rats. *Biochemical Pharmacology* **77**:1254–1265. doi:10.1016/j.bcp.2008.12.011

Cui Y, Lv G, Jin S, Peng J, Yuan J, He X, Gong H, Xu F, Xu T, Li H. 2017. A Central Amygdala-Substantia Innominata Neural Circuitry Encodes Aversive Reinforcement Signals. *Cell Rep* **21**:1770–1782. doi:10.1016/j.celrep.2017.10.062

Dave KR, Bhattacharya SK, Saul I, DeFazio RA, Dezfulian C, Lin HW, Raval AP, Perez-Pinzon MA. 2011. Activation of protein kinase C delta following cerebral ischemia leads to release of cytochrome C from the mitochondria via bad pathway. *PLoS One* **6**:e22057. doi:10.1371/journal.pone.0022057

Davis HP, Squire LR. 1984. Protein synthesis and memory: a review. *Psychol Bull* **96**:518–559.

Denton RM, Randle PJ, Martin BR. 1972. Stimulation by calcium ions of pyruvate dehydrogenase phosphate phosphatase. *The Biochemical journal* **128**:161–163. doi:10.1042/bj1280161

Dilly GA, Kittleman CW, Kerr TM, Messing RO, Mayfield RD. 2022. Cell-type specific changes in PKC-delta neurons of the central amygdala during alcohol withdrawal. *Transl Psychiatry* **12**:289. doi:10.1038/s41398-022-02063-0

Dolan M-J, Belliart-Guérin G, Bates AS, Frechter S, Lampin-Saint-Amaux A, Aso Y, Roberts RJV, Schlegel P, Wong A, Hammad A, Bock D, Rubin GM, Preat T, Plaçais P-Y, Jefferis GSXE. 2018. Communication from Learned to Innate Olfactory Processing Centers Is Required for Memory Retrieval in Drosophila. *Neuron* **100**:651-668.e8. doi:10.1016/j.neuron.2018.08.037

Du Y, Zhao Y, Li C, Zheng Q, Tian J, Li Z, Huang TY, Zhang W, Xu H. 2018. Inhibition of PKCδ reduces amyloid-β levels and reverses Alzheimer disease phenotypes. *Journal of Experimental Medicine* **215**:1665–1677. doi:10.1084/jem.20171193

Duquesnes N, Lezoualc'h F, Crozatier B. 2011. PKC-delta and PKC-epsilon: Foes of the same family or strangers? *Journal of Molecular and Cellular Cardiology* **51**:665–673. doi:10.1016/j.yjmcc.2011.07.013

Gervasi N, Tchénio P, Preat T. 2010. PKA Dynamics in a Drosophila Learning Center: Coincidence Detection by Rutabaga Adenylyl Cyclase and Spatial Regulation by Dunce Phosphodiesterase. *Neuron* **65**:516–529. doi:10.1016/j.neuron.2010.01.014

Glancy B, Balaban RS. 2012. Role of Mitochondrial Ca2+ in the Regulation of Cellular Energetics. *Biochemistry* **51**:2959–2973. doi:10.1021/bi2018909

Glas A, Hübener M, Bonhoeffer T, Goltstein PM. 2021. Spaced training enhances memory and prefrontal ensemble stability in mice. *Current Biology* **31**:4052-4061.e6. doi:10.1016/j.cub.2021.06.085

Groessl F, Munsch T, Meis S, Griessner J, Kaczanowska J, Pliota P, Kargl D, Badurek S, Kraitsy K, Rassoulpour A, Zuber J, Lessmann V, Haubensak W. 2018. Dorsal tegmental dopamine neurons gate associative learning of fear. *Nat Neurosci* **21**:952–962. doi:10.1038/s41593-018-0174-5

Gruart A, Sciarretta C, Valenzuela-Harrington M, Delgado-García JM, Minichiello L. 2007. Mutation at the TrkB PLCγ-docking site affects hippocampal LTP and associative learning in conscious mice. *Learn Mem* **14**:54–62. doi:10.1101/lm.428307

Hamada FN, Rosenzweig M, Kang K, Pulver SR, Ghezzi A, Jegla TJ, Garrity PA. 2008. An internal thermal sensor controlling temperature preference in Drosophila. *Nature* **454**:217–220. doi:10.1038/nature07001

Haubensak W, Kunwar PS, Cai H, Ciocchi S, Wall NR, Ponnusamy R, Biag J, Dong H-W, Deisseroth K, Callaway EM, Fanselow MS, Lüthi A, Anderson DJ. 2010. Genetic dissection of an amygdala microcircuit that gates conditioned fear. *Nature* **468**:270–276. doi:10.1038/nature09553

Heisenberg M. 2003. Mushroom body memoir: From maps to models. *Nature Reviews Neuroscience* **4**:266–275. doi:10.1038/nrn1074

Helmstetter FJ, Parsons RG, Gafford GM. 2008. Macromolecular synthesis, distributed synaptic plasticity, and fear conditioning. *Neurobiol Learn Mem* **89**:324–337. doi:10.1016/j.nlm.2007.09.002

Hige T. 2018. What can tiny mushrooms in fruit flies tell us about learning and memory? *Neuroscience Research*, Achievements of Japan neuroscience award winners **129**:8–16. doi:10.1016/j.neures.2017.05.002

Himmelreich S, Masuho I, Berry JA, MacMullen C, Skamangas NK, Martemyanov KA, Davis RL. 2017. Dopamine Receptor DAMB Signals via Gq to Mediate Forgetting in Drosophila. *Cell Reports* **21**:2074–2081. doi:10.1016/j.celrep.2017.10.108

Hurley JH, Grobler JA. 1997. Protein kinase C and phospholipase C: Bilayer interactions and regulation. *Current Opinion in Structural Biology* **7**:557–565. doi:10.1016/S0959-440X(97)80122-4

Inagaki K, Chen L, Ikeno F, Lee FH, Imahashi K, Bouley DM, Rezaee M, Yock PG, Murphy E, Mochly-Rosen D. 2003. Inhibition of δ-Protein Kinase C Protects Against Reperfusion Injury of the Ischemic Heart In Vivo. *Circulation* **108**:2304–2307. doi:10.1161/01.CIR.0000101682.24138.36

Jacob PF, Waddell S. 2020. Spaced Training Forms Complementary Long-Term Memories of Opposite Valence in Drosophila. *Neuron* **106**:977-991.e4. doi:10.1016/j.neuron.2020.03.013

Jarome TJ, Helmstetter FJ. 2014. Protein degradation and protein synthesis in long-term memory formation. *Front Mol Neurosci* **7**:61. doi:10.3389/fnmol.2014.00061

Jin LQ, Wang HY, Friedman E. 2001. Stimulated D(1) dopamine receptors couple to multiple Galpha proteins in different brain regions. *J Neurochem* **78**:981–990. doi:10.1046/j.1471-4159.2001.00470.x

Kajimoto T, Sawamura S, Tohyama Y, Mori Y, Newton AC. 2010. Protein kinase C {delta}-specific activity reporter reveals agonist-evoked nuclear activity controlled by Src family of kinases. *J Biol Chem* **285**:41896–41910. doi:10.1074/jbc.M110.184028

Kaul S, Anantharam V, Yang Y, Choi CJ, Kanthasamy A, Kanthasamy AG. 2005. Tyrosine phosphorylation regulates the proteolytic activation of protein kinase Cdelta in dopaminergic neuronal cells. *J Biol Chem* **280**:28721–28730. doi:10.1074/jbc.M501092200

Kim Y-K, Hammerling U. 2020. The mitochondrial PKCδ/retinol Signal Complex exerts real-time Control on Energy Homeostasis. *Biochim Biophys Acta Mol Cell Biol Lipids* **1865**:158614. doi:10.1016/j.bbalip.2020.158614

Lavington E, Cogni R, Kuczynski C, Koury S, Behrman EL, O'Brien KR, Schmidt PS, Eanes WF. 2014. A small system--high-resolution study of metabolic adaptation in the central metabolic pathway to temperate climates in Drosophila melanogaster. *Mol Biol Evol* **31**:2032–2041. doi:10.1093/molbev/msu146

Liu C, Plaçais P-Y, Yamagata N, Pfeiffer BD, Aso Y, Friedrich AB, Siwanowicz I, Rubin GM, Preat T, Tanimoto H. 2012. A subset of dopamine neurons signals reward for odour memory in Drosophila. *Nature* **488**:512–516. doi:10.1038/nature11304

Lutas A, Wahlmark CJ, Acharjee S, Kawasaki F. 2012. Genetic Analysis in Drosophila Reveals a Role for the Mitochondrial Protein P32 in Synaptic Transmission. *G3 (Bethesda)* **2**:59–69. doi:10.1534/g3.111.001586

McGuire SE, Le PT, Osborn AJ, Matsumoto K, Davis RL. 2003. Spatiotemporal rescue of memory dysfunction in Drosophila. *Science* **302**:1765–1768. doi:10.1126/science.1089035

Mery F, Kawecki TJ. 2005. A Cost of Long-Term Memory in Drosophila. *Science* **308**:1148–1148. doi:10.1126/science.1111331

Ming Y, Zhang H, Long L, Wang F, Chen J, Zhen X. 2006. Modulation of Ca2+ signals by phosphatidylinositol-linked novel D1 dopamine receptor in hippocampal neurons. *Journal of Neurochemistry* **98**:1316–1323. doi:10.1111/j.1471-4159.2006.03961.x

Minichiello L, Calella AM, Medina DL, Bonhoeffer T, Klein R, Korte M. 2002. Mechanism of TrkB-mediated hippocampal long-term potentiation. *Neuron* **36**:121–137. doi:10.1016/s0896-6273(02)00942-x

Mizuno N, Itoh H. 2009. Functions and Regulatory Mechanisms of Gq-Signaling Pathways. *Neurosignals* **17**:42–54. doi:10.1159/000186689

Mustard JA, Beggs KT, Mercer AR. 2005. Molecular biology of the invertebrate dopamine receptors. *Arch Insect Biochem Physiol* **59**:103–117. doi:10.1002/arch.20065

Nishijima S, Maruyama IN. 2017. Appetitive Olfactory Learning and Long-Term Associative Memory in Caenorhabditis elegans. *Front Behav Neurosci* **11**:80. doi:10.3389/fnbeh.2017.00080

Padamsey Z, Rochefort NL. 2023. Paying the brain's energy bill. *Current Opinion in Neurobiology* **78**:102668. doi:10.1016/j.conb.2022.102668

Pascual A, Préat T. 2001. Localization of long-term memory within the Drosophila mushroom body. *Science* **294**:1115–1117. doi:10.1126/science.1064200

Phan TG, Wright PM, Markus R, Howells DW, Davis SM, Donnan GA. 2002. Salvaging the ischaemic penumbra: more than just reperfusion? *Clin Exp Pharmacol Physiol* **29**:1–10. doi:10.1046/j.1440-1681.2002.03609.x

Plaçais PY, De Tredern É, Scheunemann L, Trannoy S, Goguel V, Han KA, Isabel G, Preat T. 2017. Upregulated energy metabolism in the Drosophila mushroom body is the trigger for long-term memory. *Nature Communications* **8**:1–14. doi:10.1038/ncomms15510

Plaçais PY, Preat T. 2013. To favor survival under food shortage, the brain disables costly memory. *Science* **339**:440–442. doi:10.1126/science.1226018

Plaçais PY, Trannoy S, Isabel G, Aso Y, Siwanowicz I, Belliart-Guérin G, Vernier P, Birman S, Tanimoto H, Preat T. 2012. Slow oscillations in two pairs of dopaminergic neurons gate long-term memory formation in Drosophila. *Nature Neuroscience* **15**:592–599. doi:10.1038/nn.3055

Qi X, Disatnik MH, Shen N, Sobel RA, Mochly-Rosen D. 2011. Aberrant mitochondrial fission in neurons induced by protein kinase Cδ under oxidative stress conditions in vivo. *Molecular Biology of the Cell* **22**:256–265. doi:10.1091/mbc.E10-06-0551

Quinn WG, Harris WA, Benzer S. 1974. Conditioned behavior in Drosophila melanogaster. *Proceedings of the National Academy of Sciences of the United States of America* **71**:708–712. doi:10.1073/pnas.71.3.708

Rabah Y, Frances R, Plaçais P-Y, Preat T. 2022. Glycolysis-derived alanine from glia fuels neuronal mitochondria for memory in Drosophila. doi:10.1101/2022.05.30.493961

Rashid AJ, O'Dowd BF, Verma V, George SR. 2007. Neuronal Gq/11-coupled dopamine receptors: an uncharted role for dopamine. *Trends in Pharmacological Sciences* **28**:551–555. doi:10.1016/j.tips.2007.10.001

Rosato RR, Fernandez R, Paz LI, Singh CR, Rosato AE. 2014. TCA cycle-mediated generation of ROS is a key mediator for HeR-MRSA survival under β-lactam antibiotic exposure. *PLoS One* **9**:e99605. doi:10.1371/journal.pone.0099605

San Martín A, Ceballo S, Baeza-Lehnert F, Lerchundi R, Valdebenito R, Contreras-Baeza Y, Alegría K, Barros LF. 2014. Imaging mitochondrial flux in single cells with a FRET sensor for pyruvate. *PLoS ONE* **9**. doi:10.1371/journal.pone.0085780

Sara SJ. 2009. The locus coeruleus and noradrenergic modulation of cognition. *Nat Rev Neurosci* **10**:211–223. doi:10.1038/nrn2573

Scheunemann L, Plaçais P-Y, Dromard Y, Schwärzel M, Preat T. 2018. Dunce Phosphodiesterase Acts as a Checkpoint for Drosophila Long-Term Memory in a Pair of Serotonergic Neurons. *Neuron* **98**:350-365.e5. doi:10.1016/j.neuron.2018.03.032

Séjourné J, Plaçais P-Y, Aso Y, Siwanowicz I, Trannoy S, Thoma V, Tedjakumala SR, Rubin GM, Tchénio P, Ito K, Isabel G, Tanimoto H, Preat T. 2011. Mushroom body efferent neurons responsible for aversive olfactory memory retrieval in Drosophila. *Nat Neurosci* **14**:903–910. doi:10.1038/nn.2846

Shaughnessy JJ. 1977. Long-Term Retention and the Spacing Effect in Free-Recall and Frequency Judgments. *The American Journal of Psychology* **90**:587–598. doi:10.2307/1421733

Silva B, Mantha OL, Schor J, Pascual A, Plaçais P-Y, Pavlowsky A, Preat T. 2022. Glia fuel neurons with locally synthesized ketone bodies to sustain memory under starvation. *Nat Metab* **4**:213–224. doi:10.1038/s42255-022-00528-6

Sinenko SA, Starkova TYu, Kuzmin AA, Tomilin AN. 2021. Physiological Signaling Functions of Reactive Oxygen Species in Stem Cells: From Flies to Man. *Frontiers in Cell and Developmental Biology* **9**.

So CH, Verma V, Alijaniaram M, Cheng R, Rashid AJ, O'Dowd BF, George SR. 2009. Calcium Signaling by Dopamine D5 Receptor and D5-D2 Receptor Hetero-Oligomers Occurs by a Mechanism Distinct from That for Dopamine D1-D2 Receptor Hetero-Oligomers. *Mol Pharmacol* **75**:843–854. doi:10.1124/mol.108.051805

Soltoff SP. 2007. Rottlerin: an inappropriate and ineffective inhibitor of PKCdelta. *Trends Pharmacol Sci* **28**:453–458. doi:10.1016/j.tips.2007.07.003

Souza-Braga P, Lorena FB, Nascimento BPP, Marcelino CP, Ravache TT, Ricci E, Bernardi MM, Ribeiro MO. 2018. Adrenergic receptor β3 is involved in the memory consolidation process in mice. *Braz J Med Biol Res* **51**:e7564. doi:10.1590/1414-431X20187564

Steinberg EE, Gore F, Heifets BD, Taylor MD, Norville ZC, Beier KT, Földy C, Lerner TN, Luo L, Deisseroth K, Malenka RC. 2020. Amygdala-Midbrain Connections Modulate Appetitive and Aversive Learning. *Neuron* **106**:1026-1043.e9. doi:10.1016/j.neuron.2020.03.016

Sutton MA, Ide J, Masters SE, Carew TJ. 2002. Interaction between amount and pattern of training in the induction of intermediate- and long-term memory for sensitization in aplysia. *Learn Mem* **9**:29–40. doi:10.1101/lm.44802

Tully T, Preat T, Boynton SC, Del Vecchio M. 1994. Genetic dissection of consolidated memory in Drosophila. *Cell* **79**:35–47. doi:10.1016/0092-8674(94)90398-0

Turrel O, Goguel V, Preat T. 2018. Amnesiac Is Required in the Adult Mushroom Body for Memory Formation. *J Neurosci* **38**:9202–9214. doi:10.1523/JNEUROSCI.0876-18.2018

Van Der Zee EA, Douma BRK. 1997. Historical review of research on protein kinase C in learning and memory. *Prog Neuro Psychopharmacol & Bio Psychiat*. doi:10.1017/CBO9781107415324.004

Wang Xinxin, Zhang Y, Wang Xu, Dai J, Hua R, Zeng S, Li H. 2020. Anxiety-related cell-type-specific neural circuits in the anterior-dorsal bed nucleus of the stria terminalis. *Science Bulletin* **65**:1203–1216. doi:10.1016/j.scib.2020.03.028

Wilensky AE, Schafe GE, Kristensen MP, LeDoux JE. 2006. Rethinking the Fear Circuit: The Central Nucleus of the Amygdala Is Required for the Acquisition, Consolidation, and Expression of Pavlovian Fear Conditioning. *J Neurosci* **26**:12387–12396. doi:10.1523/JNEUROSCI.4316-06.2006

Williford KM, Taylor A, Melchior JR, Yoon HJ, Sale E, Negasi MD, Adank DN, Brown JA, Bedenbaugh MN, Luchsinger JR, Centanni SW, Patel S, Calipari ES, Simerly RB, Winder DG. 2023. BNST PKCδ neurons are activated by specific aversive conditions to promote anxiety-like behavior. *Neuropsychopharmacol* **48**:1031–1041. doi:10.1038/s41386-023-01569-5

Wu-zhang AX, Murphy AN, Bachman M, Newton AC. 2012. Isozyme-specific Interaction of Protein Kinase C δ with Mitochondria Dissected Using Live Cell Fluorescence. *Journal of Biological Chemistry* **287**:37891–37906. doi:10.1074/jbc.M112.412635

Yang Y, Kaul S, Zhang D, Anantharam V, Kanthasamy AG. 2004. Suppression of caspase-3-dependent proteolytic activation of protein kinase C delta by small interfering RNA prevents MPP+-induced dopaminergic degeneration. *Mol Cell Neurosci* **25**:406–421. doi:10.1016/j.mcn.2003.11.011

Young MB, Thomas SA. 2014. M_1-Muscarinic Receptors Promote Fear Memory Consolidation via Phospholipase C and the M-Current. *J Neurosci* **34**:1570–1578. doi:10.1523/JNEUROSCI.1040-13.2014

Yu D, Akalal D-BG, Davis RL. 2006. Drosophila α/β Mushroom Body Neurons Form a Branch-Specific, Long-Term Cellular Memory Trace After Spaced Olfactory Conditioning. *Neuron* **52**:845–855. doi:10.1016/j.neuron.2006.10.030

Zafiri D, Duvarci S. 2022. Dopaminergic circuits underlying associative aversive learning. *Front Behav Neurosci* **16**:1041929. doi:10.3389/fnbeh.2022.1041929

Zaja I, Bai X, Liu Y, Kikuchi C, Dosenovic S, Yan Y, Canfield SG, Bosnjak ZJ. 2014. Cdk1, PKCδ and calcineurin-mediated Drp1 pathway contributes to mitochondrial fission-induced cardiomyocyte death. *Biochemical and Biophysical Research Communications* **453**:710–721. doi:10.1016/j.bbrc.2014.09.144

Zhang D, Anantharam V, Kanthasamy A, Kanthasamy AG. 2007. Neuroprotective effect of protein kinase C delta inhibitor rottlerin in cell culture and animal models of Parkinson's disease. *J Pharmacol Exp Ther* **322**:913–922. doi:10.1124/jpet.107.124669

Zhang J, Wang X, Vikash V, Ye Q, Wu D, Liu Y, Dong W. 2016. ROS and ROS-Mediated Cellular Signaling. *Oxidative Medicine and Cellular Longevity* **2016**:e4350965. doi:10.1155/2016/4350965

925 **Figures**

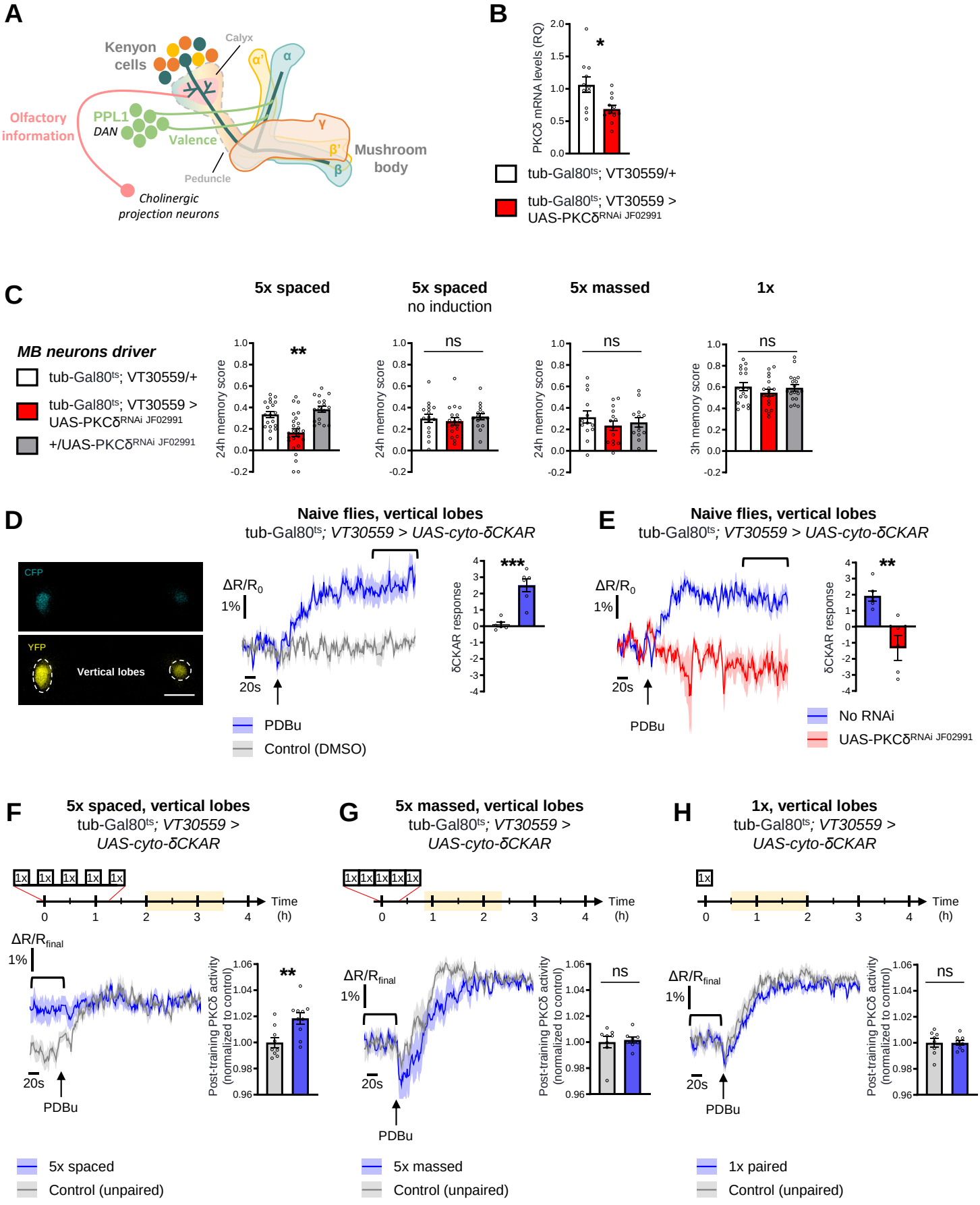
A
Kenyon cells
Calyx
α'
α
γ
Olfactory information
PPL1
DAN
Valence
γ
β'
β
Mushroom body
Peduncle
Cholinergic projection neurons
B
PKCδ mRNA levels (RQ)
tub-Gal80ts; VT30559/+
tub-Gal80ts; VT30559 > UAS-PKCδRNAi JF02991
C
5x spaced
5x spaced no induction
5x massed
1x
MB neurons driver
tub-Gal80ts; VT30559/+
tub-Gal80ts; VT30559 > UAS-PKCδRNAi JF02991
+/UAS-PKCδRNAi JF02991
24h memory score
3h memory score
ns
D
Naive flies, vertical lobes
tub-Gal80ts; VT30559 > UAS-cyto-δCKAR
CFP
YFP
Vertical lobes
ΔR/R0
1%
20s
PDBu
Control (DMSO)
δCKAR response
E
Naive flies, vertical lobes
tub-Gal80ts; VT30559 > UAS-cyto-δCKAR
No RNAi
UAS-PKCδRNAi JF02991
F
5x spaced, vertical lobes
tub-Gal80ts; VT30559 > UAS-cyto-δCKAR
Time (h)
ΔR/Rfinal
Post-training PKCδ activity (normalized to control)
5x spaced
Control (unpaired)
G
5x massed, vertical lobes
tub-Gal80ts; VT30559 > UAS-cyto-δCKAR
5x massed
Control (unpaired)
H
1x, vertical lobes
tub-Gal80ts; VT30559 > UAS-cyto-δCKAR
1x paired
Control (unpaired)

Figure 1. PKCδ is required in MB neurons for LTM formation.

(A) Schematic representation of Drosophila MB. The MB includes ~2,000 intrinsic neurons per brain hemisphere. Their cell bodies are located in the dorsal posterior part of the brain. MB neurons each send a single neurite into the neuropil, which first traverses the calyx, a dendritic region where MB neurons receive olfactory input from projections neurons, and then extends into a long axonal branch. The bundled axons of MB neurons form a fascicle called the peduncle, which traverses the brain to the anterior part, where axons branch to form horizontal and vertical lobes according to three major branching patterns – α/β, α'/β' and γ (Aso et al., 2014) – that define as many neuronal categories. The MB lobes receive input from dopaminergic neurons (the DANs), which signal stimuli of positive and negative valences in a region-specific manner (Aso et al., 2014). During associative learning, dopamine release on coincidentally odorant-activated MB output synapses modulates the synaptic drive to the network of MB output neurons, which bias subsequent odor-driven behavior (Heisenberg, 2003; Hige, 2018). Aversive LTM induced by spaced training is more specifically encoded within the α/β neurons (Pascual and Préat, 2001; Séjourné et al., 2011; Yu et al., 2006), and we previously showed that LTM retrieval involves the depression of an attraction-mediated pathway efferent from the MB vertical lobes (Aso et al., 2014; Bouzaiane et al., 2015; Dolan et al., 2018; Séjourné et al., 2011). However, according to another recent study, LTM retrieval mobilizes in parallel another MB output circuit efferent from the medial lobes (Jacob and Waddell, 2020). **(B)** Expression of PKCδ RNAi in adult MB neurons induced a significant reduction in the mRNA level of PKCδ measured by RT-qPCR in fly heads. Relative Quantification (RQ) was performed, indicating the foldchange of mRNA levels relative to the control genotype (n=11, t_{20}=2,826, p=0.0104). **(C)** PKCδ knockdown in adult MB neurons impaired memory after 5x spaced conditioning (n=17-25, $F_{2,58}$=12.59, p<0.0001). Without the induction of PKCδ RNAi expression, memory formed after 5x spaced conditioning was normal (n=15-17, $F_{2,45}$=0.4100, p=0.6661). Memory formed after 5x massed training (n=13-14, $F_{2,37}$=0.6511, p=0.5273) and 1x training (n=18, $F_{2,51}$=0.8135, p=0.4490) was normal in flies knocked down for PKCδ in adult MB neurons. **(D)** The cyto-δCKAR sensor was expressed in adult MB neurons and visualized in the CFP and YFP channels. Cytosolic PKCδ activity levels are recorded within the vertical lobes of the MBs (indicated with dashed line). Scale bar=50 µm. In naïve flies, application of 250 µM of PDBu (black arrow), a pharmacological activator of PKCδ, resulted in the increase of the cyto-δCKAR response, reaching a plateau, as compared to the DMSO control (n=6, t_{10}=5.658, p=0.0002). Quantification of the mean cyto-δCKAR

response was performed 280 s after PDBu application on a time window of 560 s (black line). **(E)** In naïve flies, application of 250 µM of PDBu (black arrow) resulted in an increase in the cyto-δCKAR response that is abolished when PKCδ is knocked down in adult MB neurons (n=5-6, t_9=4.182, p=0.0024). Quantification of the mean cyto-δCKAR response was performed 280 s after PDBu application on a time window of 560 s (black line). **(F)** To compare post-conditioning cytosolic PKCδ activities (between 30 min and 1 h 30 min post-conditioning, in yellow on the imaging time frame), cyto-δCKAR traces were normalized to the plateau value reached after addition of PDBu (saturation of the sensor), thus the activity level of cytosolic PKCδ is estimated as the cyto-δCKAR signal value before PDBu application. Cytosolic PKCδ activity is increased in the vertical lobes after 5x spaced associative paired conditioning as compared to a non-associative spaced conditioning (unpaired) protocol (n=9-10, t_{17}=3.178, p=0.0055). Quantification of the mean post-training PKCδ activity was performed on a time window of 120 s before PDBu application (black line). **(G)** After 5x massed paired conditioning, cytosolic PKCδ activity was not changed as compared to 5x massed unpaired conditioning (n=8, t_{14}=0.3282, p=0.7476). **(H)** Similarly, after 1x paired conditioning, cytosolic PKCδ activity was not changed as compared to 1x unpaired conditioning (n=8, t_{14}=0.004121, p=0.9968). Data are expressed as mean ± SEM with dots as individual values, and were analyzed by one-way ANOVA with post hoc testing by the Tukey pairwise comparisons test (C) or by unpaired two-sided t-test (B, D-H). Asterisks refer to the least significant P-value of post hoc comparison between the genotype of interest and the genotypic controls (C), or to the P-value of the unpaired t-test comparison (B, D-H) using the following nomenclature: *p<0.05, **p<0.01, ***p<0.001, ns: not significant, p>0.05. See also Figure 1 – supplement 1 and Supplementary Table 1.

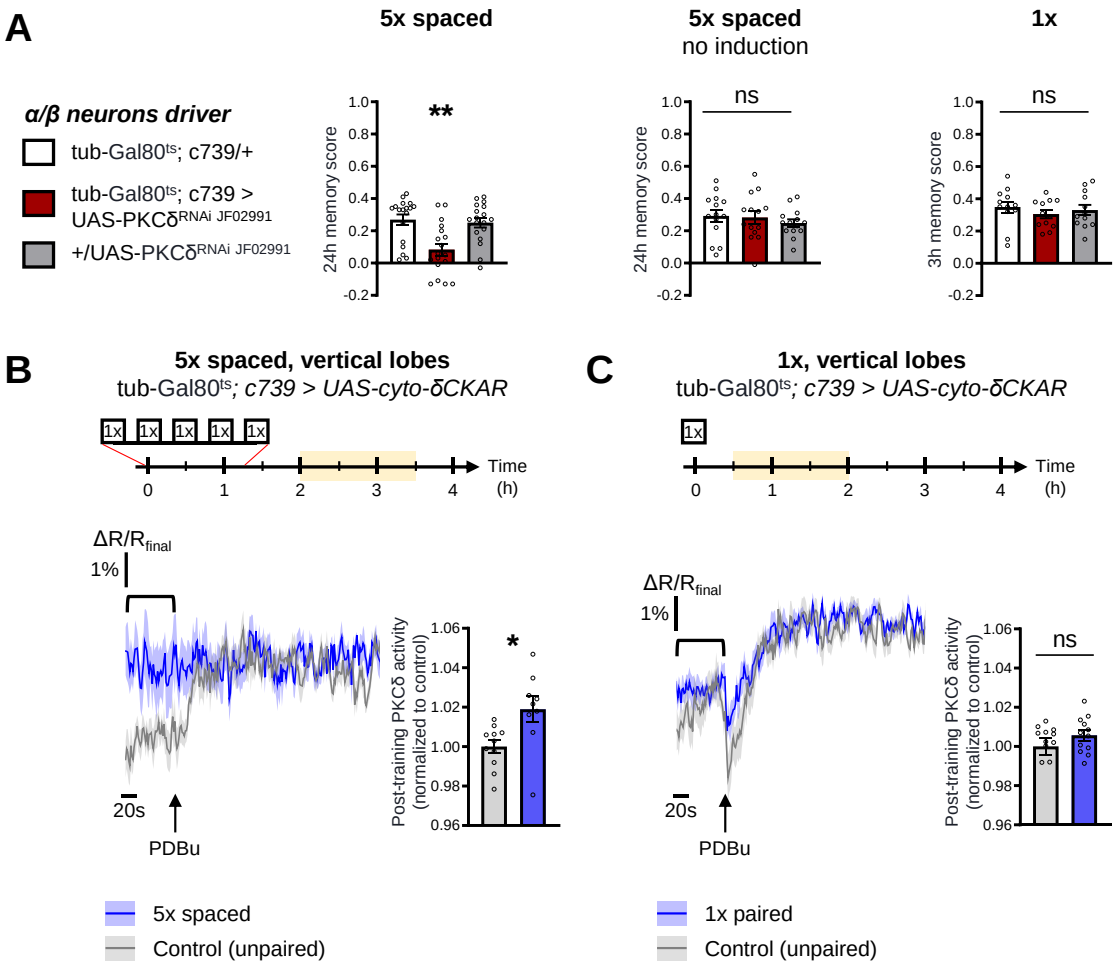

982 **Figure 2. PKCδ is required in α/β neurons for LTM formation.**

983 **(A)** When PKCδ was knocked down specifically in the α/β neurons of MBs, memory after 5x
984 spaced conditioning was impaired (n=18, $F_{2,51}$=9.521, p=0.0003). Without PKCδ RNAi
985 induction, memory after 5x spaced conditioning was normal (n=14, $F_{2,39}$=0.4673, p=0.6301).
986 Memory was also normal after 5x massed training (n=18, $F_{2,51}$=1.771, p=0.1805) and 1x
987 training (n=12, $F_{2,33}$=0.5069, p=0.6070) in flies expressing PKCδ RNAi in adult α/β MB
988 neurons. **(B)** Using the same approach as detailed in Figure 1F, the post-training activity of
989 cytosolic PKCδ was measured specifically in the α/β neurons, between 30 min and 1 h 30 min
990 post-conditioning (in yellow on the imaging time frame). After 5x spaced paired conditioning,
991 cytosolic PKCδ activity was increased in the α lobes as compared to unpaired conditioning
992 (n=9-11, t_{18}=2.723, p=0.0140). **(C)** After 1x paired conditioning, cytosolic PKCδ activity was
993 not changed as compared to unpaired conditioning (n=12, t_{22}=1.159, p=0.2590). Data are
994 expressed as mean ± SEM with dots as individual values, and were analyzed by one-way
995 ANOVA with post hoc testing by the Tukey pairwise comparisons test (A) or by unpaired two-
996 sided t-test (B-C). Asterisks refer to the least significant P-value of a post hoc comparison
997 between the genotype of interest and the genotypic controls (A) or to the P-value of the unpaired
998 t-test comparison (B-C) using the following nomenclature: *p<0.05, **p<0.01, ns: not
999 significant, p>0.05. See also Figure 2 – figure supplement 1 and Supplementary Table 1.

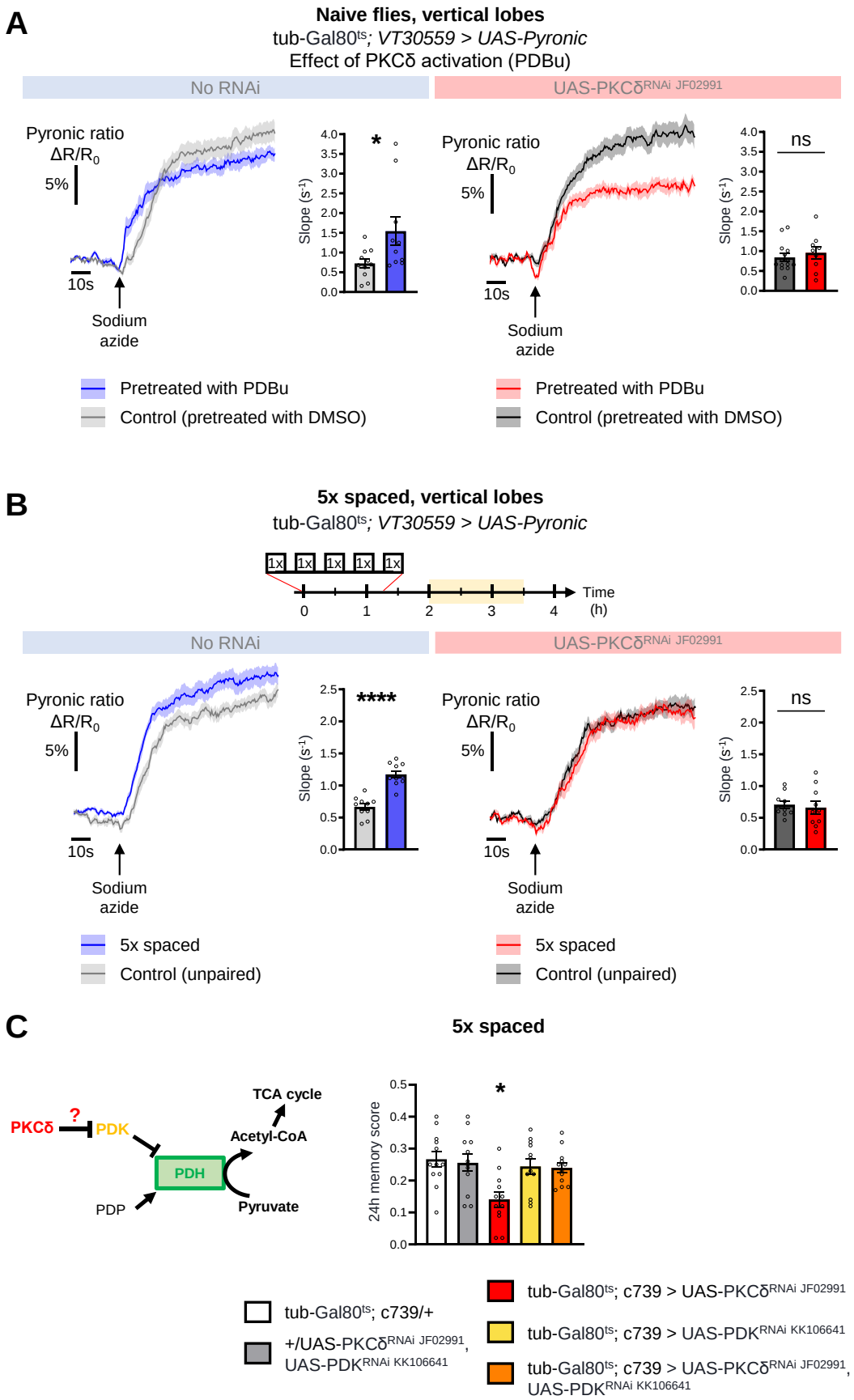

Figure 3. PKCδ regulates mitochondrial pyruvate metabolism upon LTM formation.

(A) The pyruvate sensor Pyronic was expressed in adult MB neurons and the pyruvate FRET signal was quantified in the vertical lobes. In naïve control flies (tub-Gal80^{ts}; VT30559, UAS-Pyronic), PDBu pretreatment (250 µM, 3 min) elicited a faster pyruvate accumulation following

sodium azide application (5 mM, black arrows) as compared to flies pretreated with the DMSO solvent alone (left panel, slope measurement n=10-11, t_{19}=2.311, p=0.0322). This PDBu pretreatment induced increase in pyruvate accumulation is abolished when PKCδ is knocked down in MB neurons as compared to DMSO pretreatment (right panel, slope measurement n=9-14, t_{21}=0.6734, p=0.5080). Notably, the plateaus of the pyruvate accumulation kinetics are lower when PDBu is injected onto the brains as compared to the DMSO controls. Indeed, PDBu injection is followed by a slight increase in the measured Pyronic ratio that is not sensitive to PKCδ knockdown, indicating a PDBu indirect effect independent of PKCδ on pyruvate neuronal levels (Figure 3 – figure supplement 1B). **(B)** In control flies (tub-Gal80^{ts}; VT30559, UAS-Pyronic), spaced training elicited a faster pyruvate accumulation in axons of MB neurons after sodium azide application (5 mM; black arrow) as compared to non-associative unpaired training (left panel, slope measurement n=10, t_{18}=6.751, p<0.0001). PKCδ knockdown in adult MB neurons (tub-Gal80^{ts};VT30559, UAS-Pyronic, UAS-PKCδ RNAi) impaired the spaced training induced increase in pyruvate accumulation in axons of MB neurons following sodium azide application (right panel, slope measurement n=10, t_{18}=0.3794, p=0.7089). As for Figures 1 and 2, imaging was performed between 30 min and 1 h 30 min post-conditioning, represented in yellow on the imaging time frame. **(C)** Left panel: schema of the regulation of the pyruvate dehydrogenase (PDH) complex. In mitochondria, PDHC catalyzes the conversion of pyruvate to acetyl-CoA, which enters the tricarboxylic acid cycle (TCA). PDH can be inactivated through phosphorylation by PDK. In contrast, PDP can activate a phosphorylated PDH. In our model, PKCδ regulates PDH activity via PDK inhibition. Right panel: after 5x spaced conditioning, flies coexpressing the PDK and PKCδ RNAi in the α/β MB neurons at the adult stage (tub-Gal80^{ts};c739>UAS-PKCδ RNAi, UAS-PDK RNAi) exhibited normal memory formation as compared to genotypic controls (tub-Gal80^{ts};c739/+ and +/UAS-PKCδ RNAi, UAS-PDK RNAi). Flies solely expressing the PKCδ RNAi in α/β neurons at the adult stage (tub-Gal80^{ts}; c739>UAS-PKCδ RNAi) exhibited the reported LTM defect, whereas flies that were only knocked down for PDK in adult α/β neurons (tub-Gal80^{ts};c739>UAS-PDK RNAi) formed normal memory (n=12, $F_{4,55}$=4.746, p=0.0023). Data are expressed as mean ± SEM with dots as individual values, and were analyzed by unpaired two-sided t-test (A-B) or by one-way ANOVA with post hoc testing by the Tukey pairwise comparisons test (C). Asterisks refer to the P-value of the unpaired t-test comparison or to the least significant P-value of post hoc comparison between the genotype of interest and the genotypic controls using the following nomenclature: *p<0.05, ****p<0.0001, ns: not significant, p>0.05. See also Figure 3 – figure supplement 1.

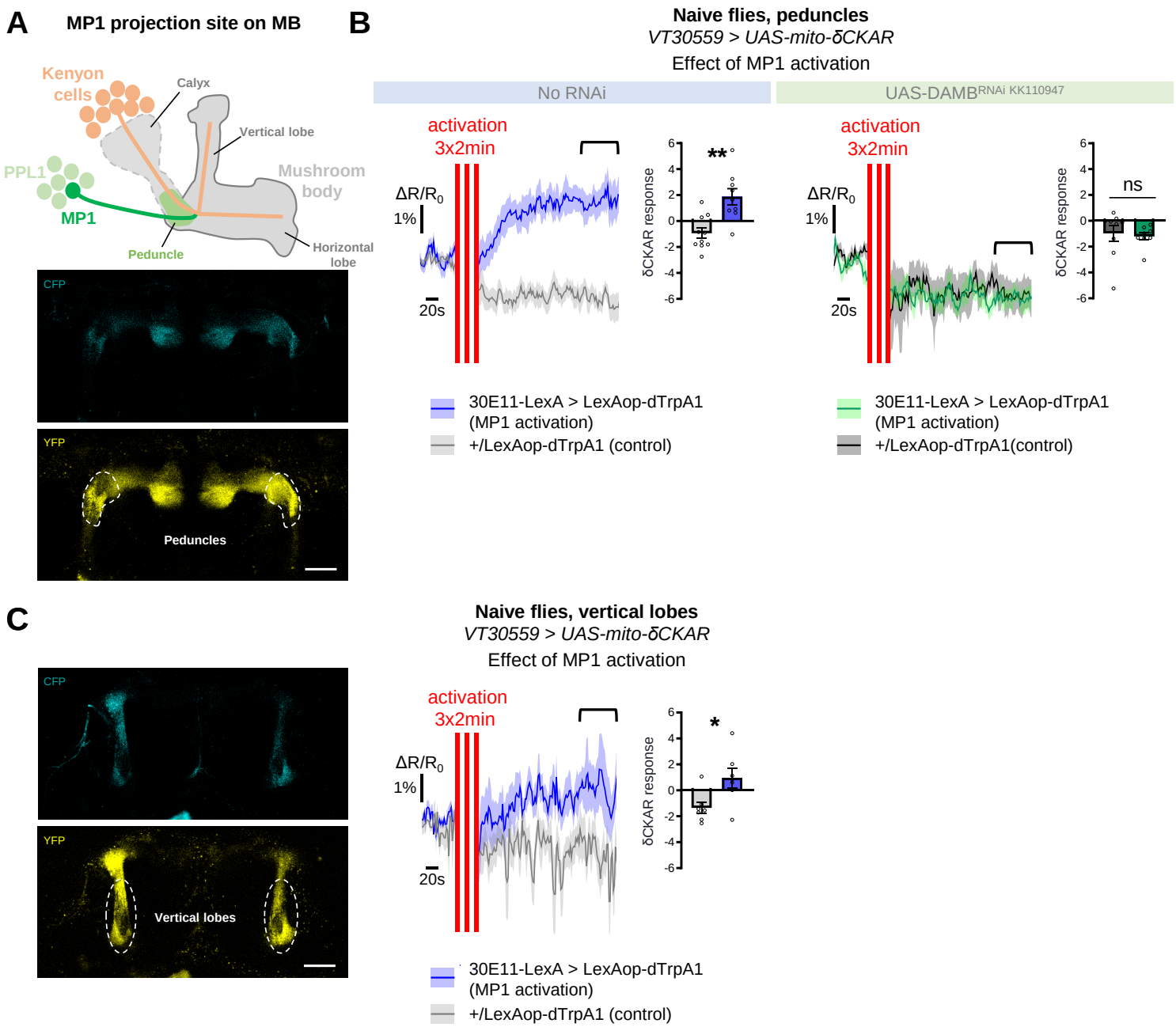

1038 **Figure 4. MP1 neurons control PKCδ activity in the MB neurons via DAMB signaling.**

1039 **(A)** Top panel: Schema of the MB structure and its afferent MP1 neuron. The dopaminergic
1040 neuron MP1 (depicted in green) in the PPL1 cluster projects onto the peduncle area of the MBs.
1041 Lower panel: The mito-δCKAR sensor was expressed in adult MB neurons and visualized in
1042 the CFP and YFP channels. The region of recording for panel B is at the level of the MB
1043 peduncles (dashed line). **(B)** Naïve flies expressing the mito-δCKAR sensor in MB neurons
1044 together with the dTrpA1 (a heat-sensitive cation channel) in MP1 neurons (30E11-LexA
1045 driver) were subjected to a thermal treatment consisting of three 2-min periods at 30°C
1046 separated by 2 min (red vertical lines); control flies expressed the mito-δCKAR in MB neurons
1047 but not the dTrpA1 channel (no 30E11-LexA driver). Mitochondrial PKCδ activity was
1048 recorded before (baseline) and immediately after the activation periods. Quantification of the

mean mito-δCKAR response was performed 120 s after the last cycle of thermal activation on a time window of 480 s (black line). In naïve flies expressing the dTrpA1 channel in MP1 neurons (30E11-LexA;VT30559 > UAS-mito-δCKAR, LexAop-dTrpA1), activation of MP1 increased mitochondrial PKCδ activity as compared to control flies (VT30559 > UAS-mito-δCKAR, LexAop-dTrpA1) (n=9-10, t_{17}=3.830, p=0.0013). When DAMB was knocked down in MB neurons (30E11-LexA;VT30559>UAS-mito-δCKAR, UAS-DAMB RNAi, LexAop-dTrpA1), MP1 activation failed to increase mitochondrial PKCδ activity as compared to control flies (VT30559>UAS-mito-δCKAR, UAS-DAMB RNAi, LexAop-dTrpA1) (n=8-9, t_{15}=0.3148, p=0.7572). **(C)** The mito-δCKAR sensor was expressed in adult MB neurons and mitochondrial PKCδ activity was recorded in the vertical lobes (dashed line). As in the peduncle region, in naïve flies expressing the dTrpA1 channel in MP1 neurons (30E11-LexA;VT30559>UAS-mito-δCKAR, LexAop-dTrpA1), activation of MP1 increased mitochondrial PKCδ activity in the vertical lobes as compared to control flies (VT30559 > UAS-mito-δCKAR, LexAop-dTrpA1) (n=7, t_{12}=2.622, p=0.0223). Data are expressed as mean ± SEM with dots as individual values and were analyzed by unpaired two-sided t-test. Asterisks refer to the P-value of the unpaired t-test comparison using the following nomenclature: *p<0.05, **p<0.01, ns: not significant, p>0.05. Scale bar=30 µm. See also Figure 4 – figure supplement 1.

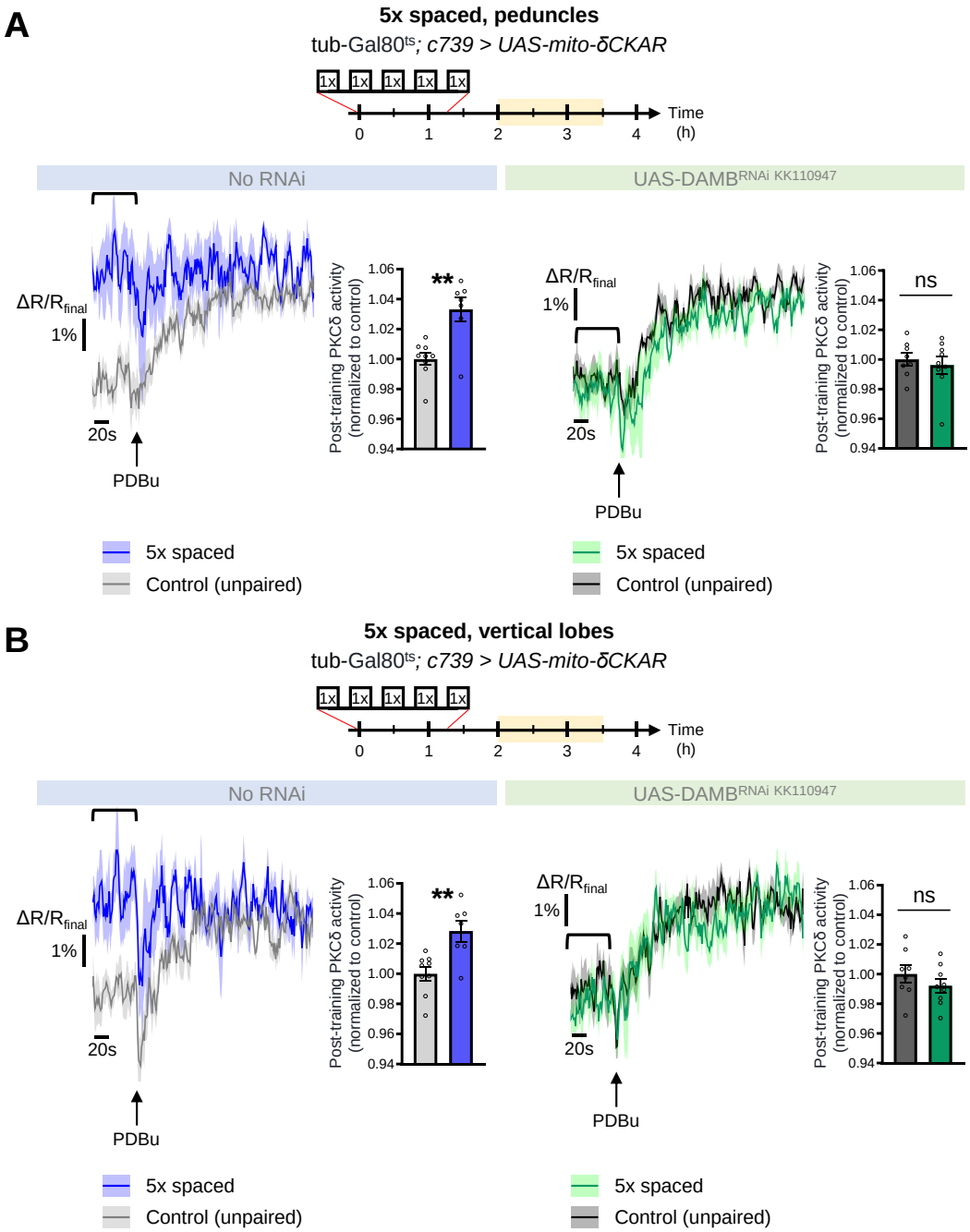

Figure 5. PKCδ translocates to the mitochondria of α/β neurons upon LTM formation.

The mito-δCKAR sensor was expressed in adult α/β neurons and the post-training activity of mito-PKCδ was measured in the peduncle **(A)** or vertical lobes **(B)**, between 30 min and 1 h 30 min post-conditioning (in yellow on the imaging time frame). The same approach was used as in Figure 1F-H with PDBu application to reach saturation level of the sensor and quantification of the mean post-training PKCδ activity performed on a time-window of 120 s before PDBu application (black line). **(A)** After 5x spaced paired conditioning, mitochondrial PKCδ activity in the peduncle was increased as compared to unpaired conditioning (left panel, n=7-9, t_{14}=3.555, p=0.0032). When DAMB was knocked down in adult α/β neurons, mitochondrial PKCδ activity was not changed after 5x spaced paired conditioning as compared to unpaired

conditioning (right panel, n=8-9, t_{15}=1.089, p=0.2934). **(B)** At the level of the vertical lobes, after 5x spaced paired conditioning, mitochondrial PKCδ activity was increased as compared to unpaired conditioning (left panel n=7-9, t_{14}=3.932, p=0.0015). When DAMB was knocked down in adult α/β neurons, mitochondrial PKCδ activity was not changed after 5x spaced paired conditioning, as compared to unpaired conditioning (right panel n=8-9, t_{15}=0.5247, p=0.6075). Data are expressed as mean ± SEM with dots as individual values, and were analyzed by unpaired two-sided t-test. Asterisks refer to the P-value of the unpaired t-test comparison using the following nomenclature: **p<0.01, ns: not significant, p>0.05.

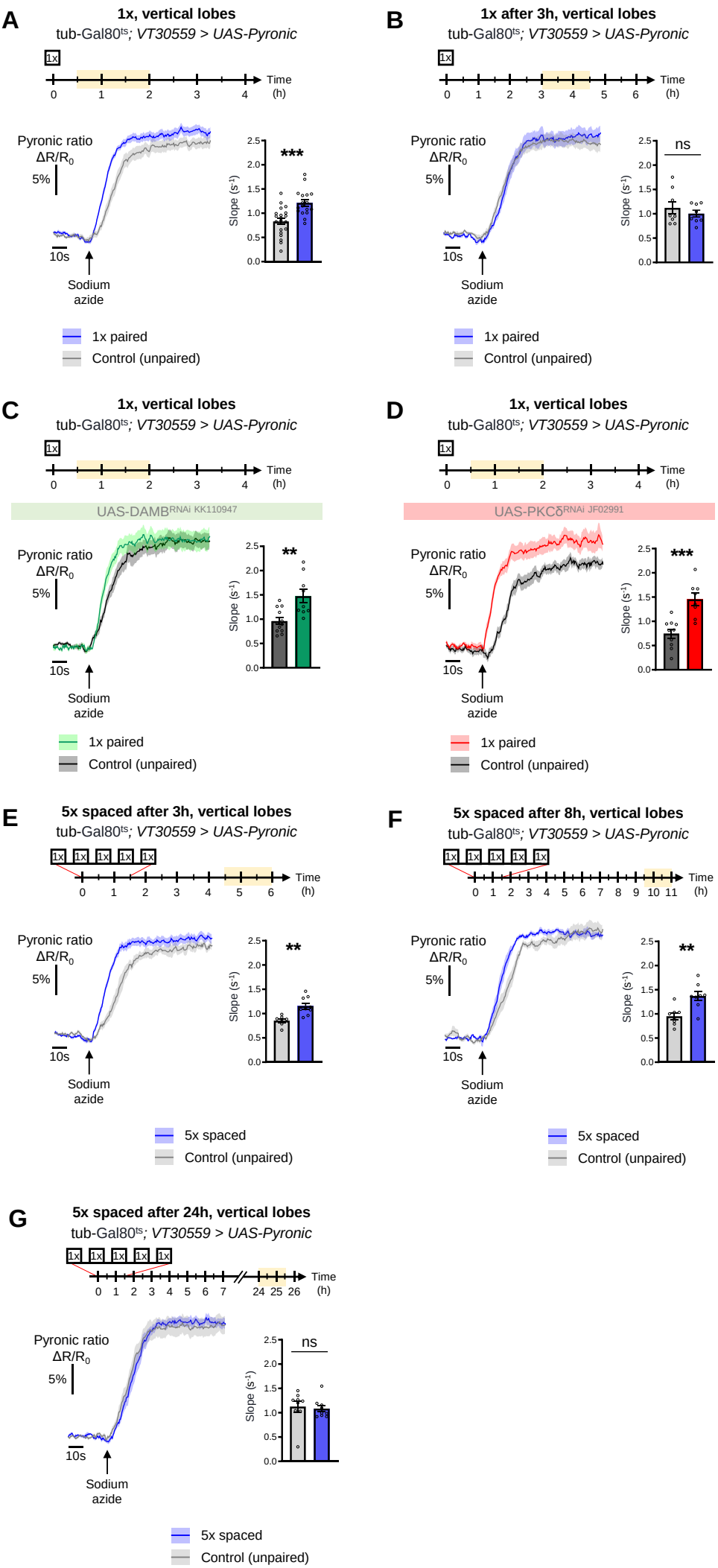
A
1x, vertical lobes
tub-Gal80ts; VT30559 > UAS-Pyronic
1x
Time (h)
0 1 2 3 4
Pyronic ratio
ΔR/R0
5%
10s
Sodium azide
Slope (s-1)
***
1x paired
Control (unpaired)
B
1x after 3h, vertical lobes
tub-Gal80ts; VT30559 > UAS-Pyronic
1x
Time (h)
0 1 2 3 4 5 6
Pyronic ratio
ΔR/R0
5%
10s
Sodium azide
Slope (s-1)
ns
1x paired
Control (unpaired)
C
1x, vertical lobes
tub-Gal80ts; VT30559 > UAS-Pyronic
1x
Time (h)
0 1 2 3 4
UAS-DAMBRNAi KK110947
Pyronic ratio
ΔR/R0
5%
10s
Sodium azide
Slope (s-1)
**
1x paired
Control (unpaired)
D
1x, vertical lobes
tub-Gal80ts; VT30559 > UAS-Pyronic
1x
Time (h)
0 1 2 3 4
UAS-PKCδRNAi JF02991
Pyronic ratio
ΔR/R0
5%
10s
Sodium azide
Slope (s-1)
***
1x paired
Control (unpaired)
E
5x spaced after 3h, vertical lobes
tub-Gal80ts; VT30559 > UAS-Pyronic
1x 1x 1x 1x 1x
Time (h)
0 1 2 3 4 5 6
Pyronic ratio
ΔR/R0
5%
10s
Sodium azide
Slope (s-1)
**
5x spaced
Control (unpaired)
F
5x spaced after 8h, vertical lobes
tub-Gal80ts; VT30559 > UAS-Pyronic
1x 1x 1x 1x 1x
Time (h)
0 1 2 3 4 5 6 7 8 9 10 11
Pyronic ratio
ΔR/R0
5%
10s
Sodium azide
Slope (s-1)
**
5x spaced
Control (unpaired)
G
5x spaced after 24h, vertical lobes
tub-Gal80ts; VT30559 > UAS-Pyronic
1x 1x 1x 1x 1x
Time (h)
0 1 2 3 4 5 6 7 24 25 26
Pyronic ratio
ΔR/R0
5%
10s
Sodium azide
Slope (s-1)
ns
5x spaced
Control (unpaired)

1085

Figure 6. The DAMB/PKCδ axis is specific to LTM formation.

The pyruvate sensor Pyronic was expressed in adult MB neurons and pyruvate accumulation was measured after conditioning in the vertical lobes. For each panel, the period of imaging after conditioning is indicated in yellow on the imaging time frame. **(A)** 30 min to 1 h 30 min after 1x paired conditioning, an increased pyruvate flux was measured in control flies (tub-Gal80^{ts};VT30559, UAS-Pyronic) as compared to non-associative unpaired 1x training (slope measurement n=17-20, t_{35}=4.075, p=0.0003). Here, we pooled the data obtained from control flies acquired in parallel to DAMB and PKCδ knockdown flies (panels C and D). **(B)** 3 h to 4 h 30 min after 1x paired conditioning of control flies (tub-Gal80^{ts};VT30559, UAS-Pyronic), the rate of pyruvate accumulation was similar as compared to unpaired conditioning (slope measurement n=8, t_{14}=0.8022, p=0.4359). **(C)** 30 min to 1 h 30 min after 1x paired conditioning, the pyruvate flux was still increased when DAMB was knocked down in the MBs at the adult stage (tub-Gal80^{ts};VT30559, UAS-Pyronic, UAS-DAMB RNAi) (slope measurement n=9-12, t_{19}=3.528, p=0.0022). **(D)** Similarly, PKCδ knockdown in adult MB neurons (tub-Gal80^{ts}; VT30559, UAS-Pyronic, UAS-PKCδ RNAi) did not impair the 1x conditioning induced increase in pyruvate accumulation in MB neuron axons (slope measurement n=8-10, t_{16}=4.568, p=0.0003). **(E)** 3 h to 4 h 30 min after the last cycle of 5x spaced conditioning of control flies (tub-Gal80^{ts};VT30559, UAS-Pyronic), the pyruvate flux was increased as compared to 5x spaced unpaired conditioning (slope measurement n=9-7, t_{14}=3.889, p=0.0016). **(F)** 8 h to 9 h 30 min after the last cycle of 5x spaced conditioning of control flies (tub-Gal80^{ts};VT30559, UAS-Pyronic), the pyruvate flux was still increased as compared to 5x spaced unpaired conditioning (slope measurement n=8, t_{14}=3.628, p=0.0027). **(G)** 24 h after the last cycle of 5x spaced conditioning of control flies (tub-Gal80^{ts};VT30559, UAS-Pyronic), the pyruvate flux was similar as compared to 5x spaced unpaired conditioning (slope measurement n=9, t_{16}=0.3256, p=0.7489). Data are expressed as mean ± SEM with dots as individual values, and were analyzed by unpaired two-sided t-test. Asterisks refer to the P-value of the unpaired t-test comparison using the following nomenclature: **p<0.01, ***p<0.001, ns: not significant, p>0.05.

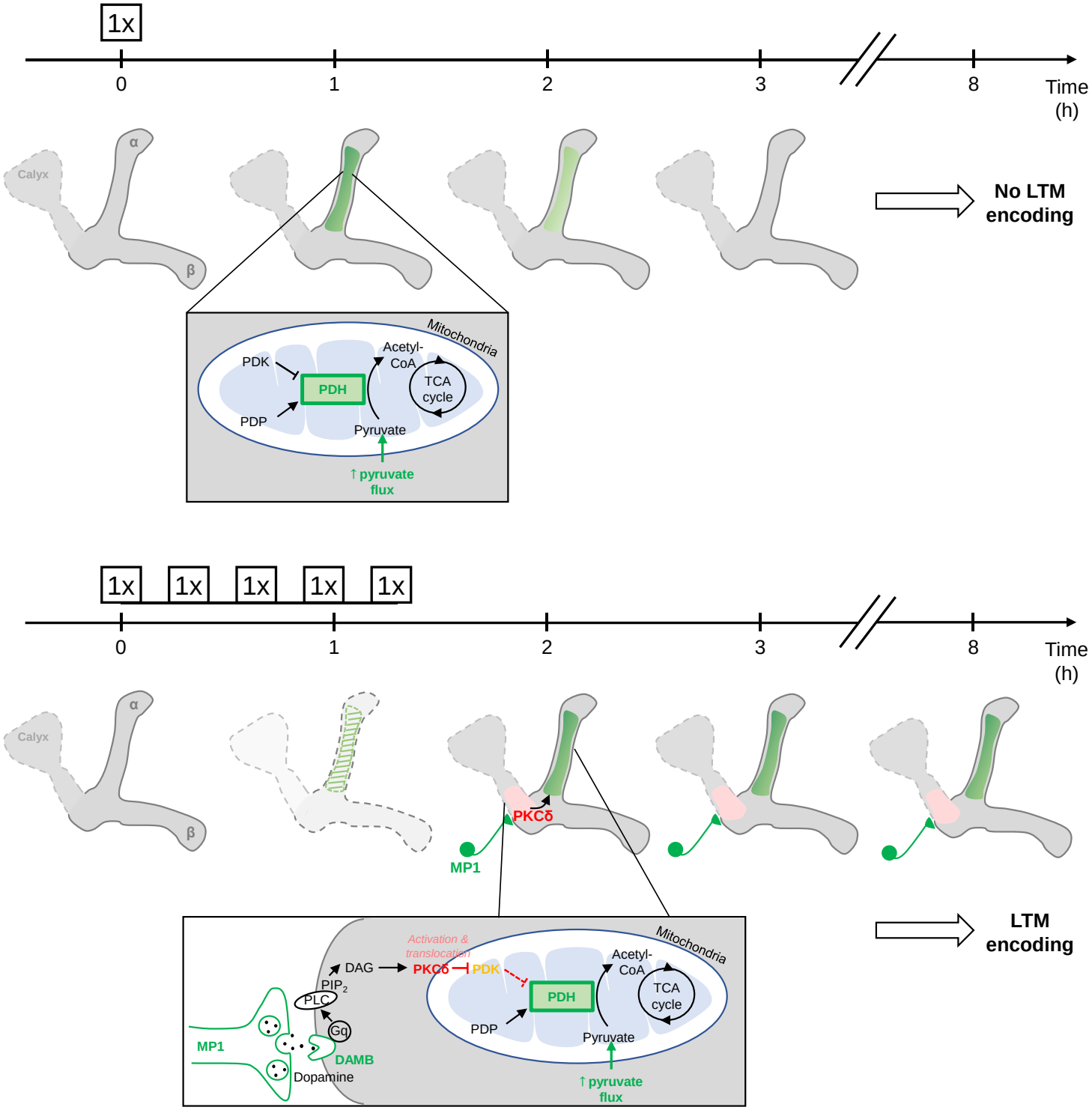

Figure 7. Schema of the energy-based gating of LTM, illustrating the role of PKCδ downstream of the DAMB signaling cascade.

After 1x training, the pyruvate flux to the mitochondria in the vertical lobes of MB neurons is increased (Rabah et al., 2022). This increased energy state is not maintained but is progressively turned off, and after 3 h, the MBs are back to their basal energy state.

Upon spaced training, in addition to the mechanism occurring after 1x training, the enhanced oscillatory activity of MP1 neurons activates DAMB signaling in the efferent α/β MB neurons.

The DAMB receptor preferentially couples with Gq and the produced DAG activates PKCδ, which results in its translocation to mitochondria. There, PKCδ can activate the PDH, by releasing the inhibition exerted by PDK. The enhanced PDH activity promotes an increase in mitochondrial pyruvate flux, and this enhanced energy state gates memory consolidation, thereby enabling LTM formation. After 3 and even 8 hours, the lasting effect of PKCδ on mitochondrial metabolism maintains the high energy state of the MBs needed to support LTM formation.

Supplemental information

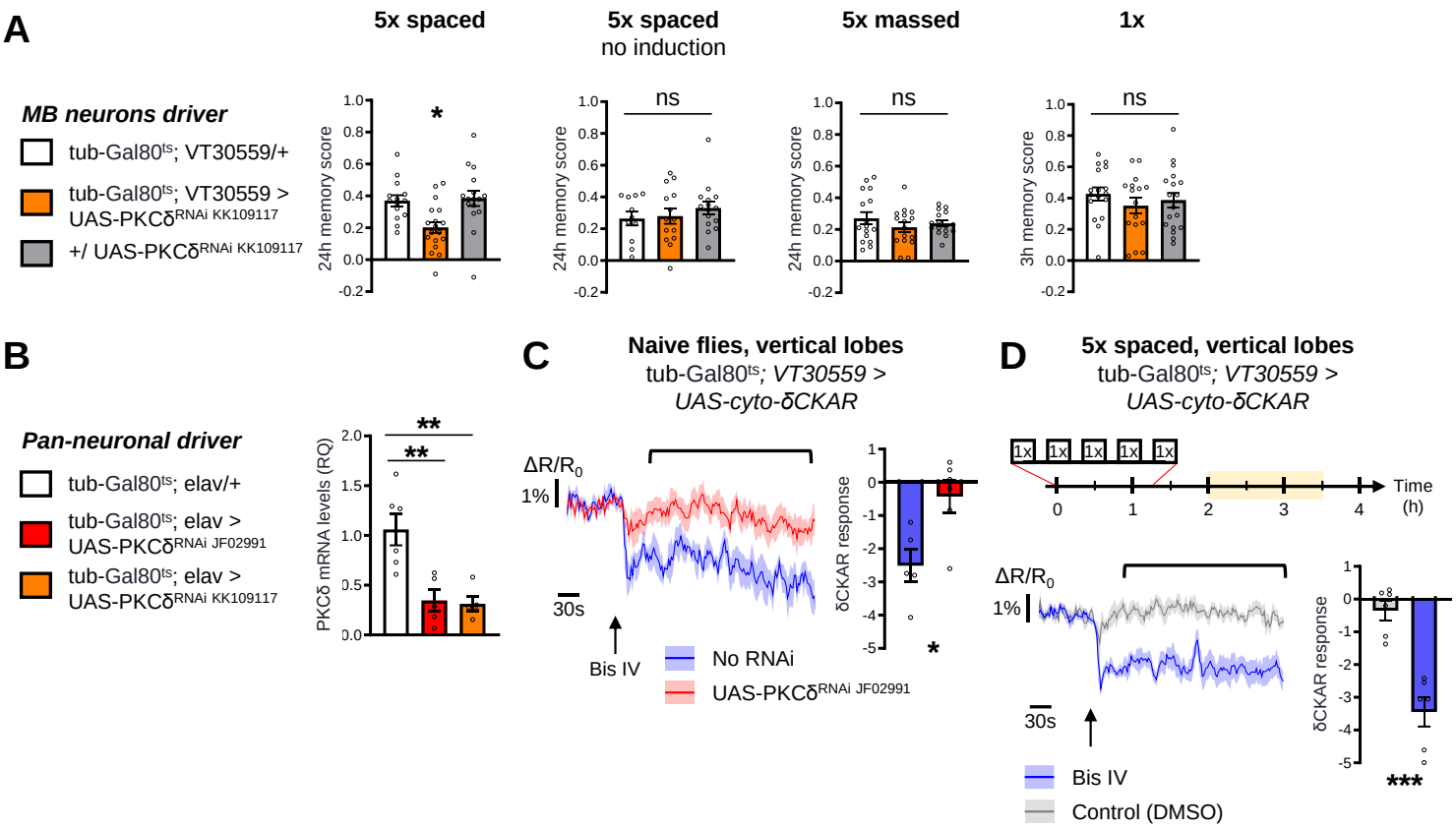

Figure 1 – figure supplement 1. Control experiments for behavior analysis and δCKAR imaging experiments.

(A) Behavior analysis with a second PKCδ RNAi: 24-h memory after 5x spaced conditioning was also specifically impaired after induction of the PKCδ RNAi expression in adult MB (n=14-18, $F_{2,45}$=6.764, p=0.027), and it was not impacted without induction (n=11-15, $F_{2,37}$=0.6226, p=0.5421). No memory defect was found after 5x massed training (n=16, $F_{2,45}$=0.8968, p=0.4151) or 1x training (n=17-18, $F_{2,48}$=0.6592, p=0.5219) in flies knocked down for PKCδ in adult MB. **(B)** Pan-neuronal expression of either PKCδ RNAi at the adult stage significantly reduced PKCδ mRNA levels. Relative Quantification (RQ) was performed, indicating the foldchange of mRNA levels relative to the control genotype (n=5-6, $F_{2,13}$=11.85, p=0.0012). **(C)** In naïve flies, application of 5 µM of Bis IV (black arrow), a PKC inhibitor, resulted in a decrease in the cyto-δCKAR response, and this response was abolished when PKCδ was knocked down (n=5-6, t_9=3.007, p=0.0148). Quantification of the mean cyto-δCKAR response was performed 20 s after Bis IV application on a time window of 250 s (black line). **(D)** After 5x spaced training, Bis IV injection also decreased the cyto-δCKAR response as compared to the DMSO control (n=6, t_{10}=4.825, p=0.0007). Data are expressed as mean ± SEM with dots

as individual values, and were analyzed either by one-way ANOVA with post hoc testing by the Tukey pairwise comparisons test (A-B), or by an unpaired two-sided t-test (C-D). Asterisks refer to the least significant P-value of post hoc comparison between the genotype of interest and the genotypic controls (A-B) or to the P-value of the unpaired t-test comparison (C-D) using the following nomenclature: *$p<0.05$, **$p<0.01$, ***$p<0.001$, ns: not significant, $p>0.05$.

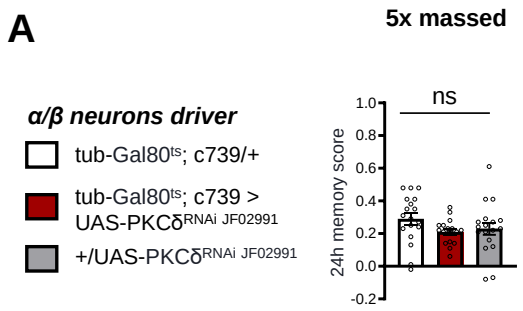

Figure 2 – figure supplement 1. Control analysis of 24-h memory formed after massed training upon PKCδ knockdown in α/β neurons.

(A) 24-h memory after 5x massed training was normal when PKCδ RNAi was expressed in the α/β neurons at the adult stage as compared to its genotypic controls (n=18, $F_{2,51}$=1.771, p=0.1805). Data are expressed as mean ± SEM with dots as individual values, and were analyzed by one-way ANOVA with post hoc testing by the Tukey pairwise comparisons test. ns: not significant, p>0.05.

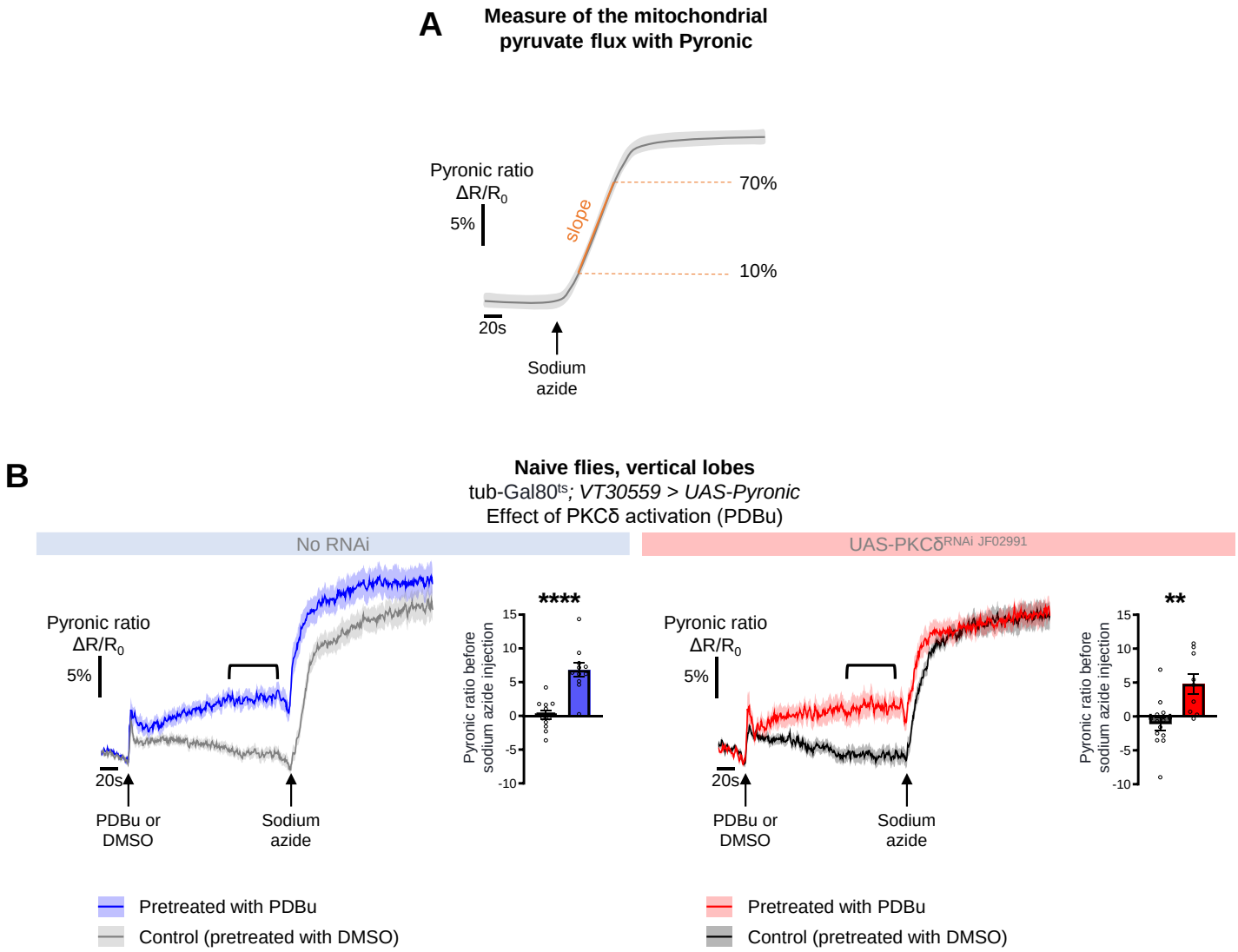

Figure 3 – figure supplement 1. Additional information on pyruvate flux measurement using the Pyronic sensor.

(A) Schema representing the measure of the mitochondrial pyruvate flux using the pyruvate FRET sensor Pyronic. Here, mitochondrial respiration is blocked by sodium azide at the beginning of the recording, thereby stopping pyruvate mitochondrial uptake. The expected kinetic of pyruvate accumulation following the azide treatment is represented in grey, showing that pyruvate accumulates from the arrest of its mitochondrial uptake until saturation of the sensor. The rate of pyruvate accumulation (i.e. the slope of the measured kinetic, measured between 10 and 70% of the plateau) reflects the rate at which pyruvate was consumed by mitochondria for energy production before their blockade. **(B)** Complete recording of pyruvate imaging data shown in Figure 3A. In control flies (tub-Gal80^{ts};VT30559, UAS-Pyronic), PDBu injection is followed by a progressive increase in the measured Pyronic ratio (black line) as compared to DMSO injection (n=11, t_{20}=5.437, p<0.0001). This effect is not sensitive to PKCδ knockdown (tub-Gal80^{ts};VT30559, UAS-Pyronic, UAS-PKCδ RNAi flies, n=9-14, t_{21}=3.542, p=0.0019). As PDBu is known to activate other PKCs (Wu-zhang et al., 2012), this observation

likely reflects a PDBu off-target effect independent of PKCδ on pyruvate neuronal levels. This effect explains why, when normalized just before azide injection (as in Figure 3A), the pyruvate accumulation plateaus appear lower when PDBu is injected onto the brains as compared to the DMSO controls. Data are expressed as mean ± SEM with dots as individual values, and were analyzed by unpaired two-sided t-test. Asterisks refer to the P-value of the unpaired t-test comparison using the following nomenclature: **$p<0.01$, ****$p<0.0001$.

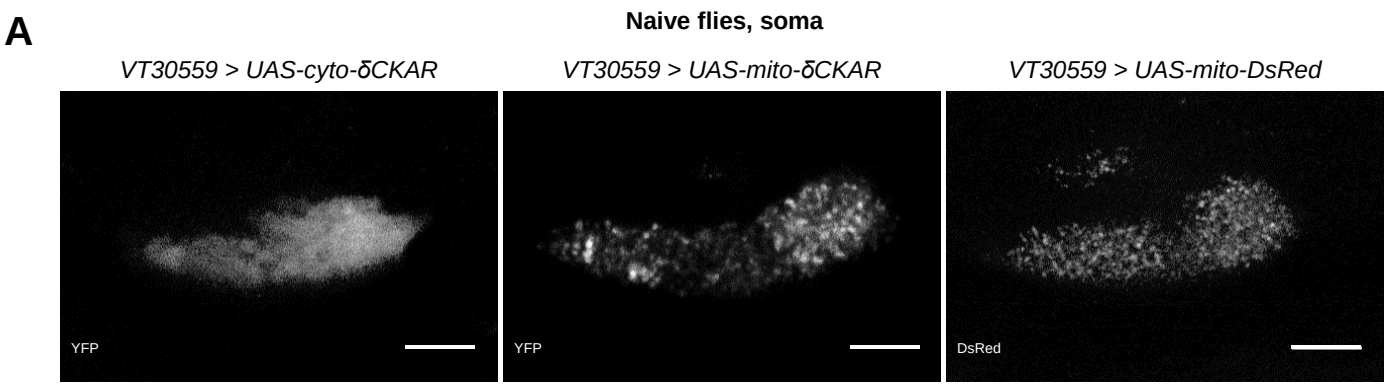

Figure 4 – figure supplement 1. Subcellular addressing of the cyto-δCKAR and mito-δCKAR probes.

(A) Comparison of fluorescence sub localization in the soma of MB neurons in flies expressing either cyto-δCKAR, mito-δCKAR or mito-DsRed (DsRed is addressed to mitochondria using the COX8 targeting sequence (Lutas et al., 2012)) under the control of the VT30559 driver. Mito-δCKAR punctate signal, similar to what is observed for mito-DsRed signal, indicates mitochondrial localization of the probe, in contrast to the diffuse signal observed with cyto-δCKAR. This comparison was done in the soma area because it is the only MB region where the density of mitochondria allows their discrimination by conventional microscopy. Images were acquired by 2-photon microscopy, cyto-and mito-δCKAR sensors were visualized through the YFP channel, and the mito-DsRed signal was acquired by 750 nm excitation and 580-610 nm detection. Scale bar=20µm.

Supplementary Table 1. Sensory acuity controls, related to Figure 1.

Genotypes	Shock Avoidance		Naive odor avoidance			
			Octanol		Methylcyclohexanol	
	Mean ± s.e.m.	Statistics	Mean ± s.e.m.	Statistics	Mean ± s.e.m.	Statistics
tubGal80^{ts};VT30559/+	0.63±0.057	$F_{2,33}$=2.60	0.74±0.053	$F_{2,27}$=5.60	0.72±0.069	$F_{2,27}$=1.27
tubGal80^{ts};VT30559>UAS-PKCδ RNAi JF02991	0.76±0.033	p=0.090	0.53±0.070	p=0.0092**	0.60±0.082	p=0.30
UAS-PKCδ RNAi JF02991/+	0.64±0.039	n=12	0.44±0.073	n=9-11	0.56±0.069	n=9-11
tubGal80^{ts};VT30559/+	0.47±0.052	$F_{2,33}$=0.38	0.63±0.040	$F_{2,33}$=2.76	0.66±0.046	$F_{2,33}$=0.64
tubGal80^{ts};VT30559>UAS-PKCδ RNAi KK109117	0.42±0.039	p=0.69	0.70±0.033	p=0.078	0.67±0.034	p=0.53
UAS-PKCδ RNAi KK109117/+	0.43±0.047	n=12	0.57±0.047	n=12	0.61±0.050	n=12
tubGal80^{ts};c739/+	0.45±0.060	$F_{2,39}$=0.61	0.58±0.050	$F_{2,33}$=2.48	0.46±0.044	$F_{2,33}$=0.94
tubGal80^{ts};c739>UAS-PKCδ RNAi JF02991	0.40±0.053	p=0.55	0.45±0.036	p=0.099	0.47±0.051	p=0.40
UAS-PKCδ RNAi JF02991/+	0.49±0.059	n=14	0.48±0.045	n=12	0.54±0.048	n=12

Control experiments for olfactory acuity and electric shock avoidance: the expression of either of the two PKCδ RNAi used in this study, in MB neurons at the adult stage had no significant effect on olfactory acuity, or on the avoidance of electric shocks.

**: Tukey post hoc comparison between the genotype of interest and controls are not significant:

tubGal80^{ts};VT30559>UAS-PKCδ RNAi JF02991 vs tubGal80^{ts}; VT30559/+ : ns

tubGal80^{ts};VT30559>UAS-PKCδ RNAi JF02991 vs UAS-PKCδ RNAi JF02991 /+ : ns

tubGal80^{ts}; VT30559/+ vs UAS-PKCδ RNAi JF02991 /+ : **